

Rheological Characterization and Modeling of Laponite Gels
with Application to Slug-like Locomotion

by

Douglas C. Hwang

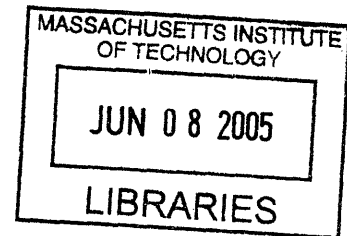
Submitted to the Department of Mechanical Engineering
in Partial Fulfillment of the Requirements for the Degree of

Bachelor of Science

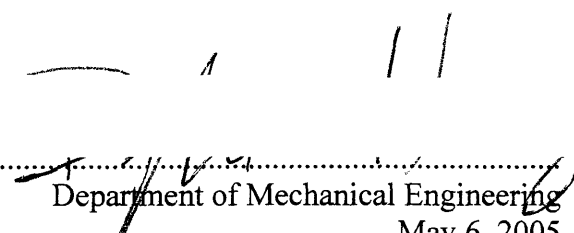
at the

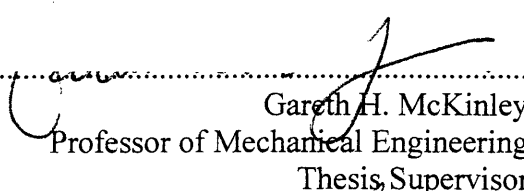
Massachusetts Institute of Technology


June 2005



© 2005 Massachusetts Institute of Technology
All rights reserved

Signature of Author 
Department of Mechanical Engineering
May 6, 2005

Certified by 
Gareth H. McKinley
Professor of Mechanical Engineering
Thesis Supervisor

Accepted by 
Professor Ernest G. Cravalho
Chairman of the Undergraduate Thesis Committee

ARCHIVES

Rheological Characterization and Modeling of Laponite Gels
with Application to Slug-like Locomotion

by

Douglas C. Hwang

Submitted to the Department of Mechanical Engineering
on May 6, 2005 in Partial Fulfillment of the Requirements
for the Degree of Bachelor of Science in
Mechanical Engineering

ABSTRACT

Using various concentrations of Laponite, results were obtained on an AR1000 rheometer through various testing methods: stress sweep, creep tests, and large amplitude oscillatory shear tests, defined as LAOS. Concentrations of 1%, 2%, 2.5%, 3%, and 4% wt. of Laponite and distilled water solutions were tested. Laponite gels over 1% wt. concentrations were characterized as yield stress materials, as determined by stress sweep, creep test, and LAOS tests. The stress sweeps determined the yield stress, and the creep tests verified the results with a range of creep tests over and below the yield stress discovered in the stress sweep tests. The LAOS tests mapped a specific “fingerprint” of how the Laponite gel behaved on a Lissajous figure of stress and strain. These LAOS results are then fit with an evolution of deformation model in Matlab over various oscillation stresses. The results show that slug slime emulation is possible by altering the Laponite gel’s properties with polymers to result in a slug slime equivalent for use in studying slug locomotion.

Thesis Supervisor: Gareth H. McKinley
Title: Professor of Mechanical Engineering

Acknowledgements

First of all, I owe a lot to Professor McKinley who has personally taught me the past 3 years at MIT, from 2.006 Thermal Fluids, to a UROP junior year, to my senior thesis. Thank to you for your patience and guidance for I was able to obtain a true educational experience at MIT. Thank you for taking as one of your students, personally investing so much time into me, being patient with me, and bringing out more potential in me than any other professor at MIT.

Suraj Deshmukh for your help in the lab, teaching me to work with all the equipment, working with me to understand my data, and teaching me the analysis needed in order to complete my thesis.

For all the memories and support the past four years, I want to give thanks to my housemates at Phi Delta Theta. And also I'd like to give recognition to all my fellow course 2 buds, whom I have shared so many suffering as well as rewarding moments with.

Thank you, Pastor Paul Becky JDSN, and the family of God at Berkland Baptist Church, thank you for your countless prayers and support over my college years at MIT. David JDSN, Angela SMN, and James hyung thank you for being such loving and caring shepherds to me, and being spiritual parents to me throughout college. As difficult as I have been to deal with, I have been the recipient for so much love, prayer, and sacrifice. ABSK staff, thank you for being older brothers and sisters in Christ and being living examples to me, teaching me to grow together in the family of God.

I want to thank my family, parents Hosuk and Eunsoo Hwang, and sister Jennifer Hwang for all their love and support throughout my college days and entire life. Thank you for sacrificing so much that I could come so far and finish MIT. Not of anything that I did, but instead all this is truly a testament of the abounding love that I have received all throughout my life.

Last, I would really like to thank Jesus Christ for being the Lord and savior of my life. Though I am thankless, undeserving, and a sinner that I've been the recipient of so much unconditional love. And most of all, for my salvation that I could have my sins forgiven so that I can have a eternal relationship with God.

But he said to me, "My grace is sufficient for you, for my power is made perfect in weakness." Therefore I will boast all the more gladly about my weaknesses, so that Christ's power may rest on me... For when I am weak, then I am strong.

2 Corinthians 12:9-10

Table of Contents

1.0 Introduction.....	19
1.1 Motivation.....	19
1.2 Goals	20
1.3 Overview.....	20
2.0 Background	22
2.1 Yield Stress	22
2.2 Material	25
2.2.1 Structure	25
2.2.2 Current Uses.....	26
2.3 Slug Locomotion.....	27
3.0 Theoretical Analysis	31
3.1 Stress Sweep and Observing Yield Stress	31
3.2 Creep and Observing Yield Stress.....	34
3.3 Large Amplitude Oscillatory Shear and Observing Yield Stress	36
4.0 Experimental Methods.....	39
4.1 Sample Preparation.....	40
4.2 Stress Sweep	41
4.3 Creep.....	43
4.4 Large Amplitude Oscillatory Shear	44
5.0 Results and Discussions.....	45

5.1 Stress Sweep	45
5.2 Creep	54
5.3 Large Amplitude Oscillatory Shear (LAOS) Tests.....	62
6.0 Conclusion	78
References.....	81
Appendix : Matlab Code Used to Fit LAOS Results on Lissajous Figures.....	84

List of Figures

Figure 1: Compares the three most used yield stress models: Bingham, Casson, and Herschel – Burkely [4]. 24

Figure 2: A three dimensional structural form of Laponite which shows the electrostatic attraction forces on the faces and edges of the surrounding Laponite crystals [7].... 26

Figure 3: Shows the size magnitude difference of Laponite compared to other colloidal suspensions, bentonite and hectorite [7]. 26

Figure 4: Illustration of how a slug contracts and expands its muscles in order to use the slug slime as a means of locomotion. 28

Figure 5: Rough diagram of a slug fixed onto a vertical wall on a layer of slug slime. ... 28

Figure 6: Theoretical hysteresis loop for a metal plotted on stress and strain axes. 32

Figure 7: Hysteresis curve of a sample fluid as the stress is swept up and down..... 33

Figure 8: Matlab graph illustrating the effect of $s = \sigma_o/\sigma_y$ on creep tests..... 34

Figure 9: Compares the Lissajous figures of $s = \sigma_o/\sigma_y < 1$, $s = \sigma_o/\sigma_y = 1$, and $s = \sigma_o/\sigma_y > 1$ using the evolution of deformation model. 38

Figure 10: AR1000 used for all the stress sweep, creep, and large amplitude oscillatory shear tests on the Laponite solutions. 39

Figure 11: A sample of 3% wt. Laponite solution upside down before being shaken, the stir bar suspended in the gel shows the elastic gel-like properties..... 41

Figure 12: A sample of 3% wt. Laponite solution, upside down after being shaken, showing the viscous fluid-like properties. 41

Figure 13: Two tests of stepped stress sweeps of a 1% wt. Laponite-water solution, showing no yield stress characteristics. 46

Figure 14: Stress sweep test of silicone oil that showing characteristics of a Newtonian fluid. 46

Figure 15: Numerous stress sweep tests stepped up and down on 2% wt. concentration of Laponite and water, showing yield stress characteristics and a hysteresis. 47

Figure 16: Numerous stress sweep tests stepped up and down on 2.5% wt. concentration of Laponite and water, showing yield stress characteristics and a hysteresis. 48

Figure 17: Numerous stress sweep tests stepped up and down on 3% wt. concentration of Laponite and water, showing yield stress characteristics and a hysteresis. 49

Figure 18: Numerous stress sweep tests stepped up and down on 4% wt. concentration of Laponite and water, showing yield stress characteristics and a hysteresis. 49

Figure 19: Semi-log scale of the 2% Laponite solution when applied a stepped stress sweep test. 51

Figure 20: Semi-log scale of the 3% Laponite solution when applied a stepped stress sweep test. 51

Figure 21: Semi-log scale of the 4% Laponite solution when applied a stepped stress sweep test. 52

Figure 22: Compendium of the stepped stress sweep curves for the 1%, 2%, 2.5%, 3% and 4% wt. Laponite solutions all at 20°C. 53

Figure 23: A comparison of the Compliance $J(t)$ for the creep tests on a 2% wt. solution of Laponite when applied shear stresses from 1 Pa to 27 Pa, showing the difference

in creep tests done with shear stresses below the yield stress and shear stresses above the yield stress value.	54
Figure 24: A comparison of the Compliance $J(t)$ for the creep tests on a 2.5% wt. solution of Laponite when applied shear stresses from 2.374 Pa to 23.57 Pa, showing the difference in creep tests with shear stresses below the yield stress value and shear stresses above the yield stress value.	55
Figure 25: A comparison of the Compliance $J(t)$ for the creep tests on a 3% wt. solution of Laponite when applied shear stresses from 15 Pa to 75 Pa, showing the difference in creep tests with shear stresses below the yield stress value and shear stresses above the yield stress value.....	56
Figure 26: A comparison of the Compliance $J(t)$ for the creep tests on a 2.5% wt. solution of Laponite when applied shear stresses from 23.57 Pa to 120 Pa, showing the difference in creep tests with shear stresses below the yield stress value and shear stresses above the yield stress value.	56
Figure 27: A fit of the creep test extracted viscosity values for a 2% wt. Laponite solution mapped onto the stepped stress sweep data for the same 2% wt. Laponite sample..	58
Figure 28: A fit of the creep extracted viscosity values for a 2.5% wt. Laponite solution mapped onto the stress sweep data for the same 2.5% wt. Laponite sample.....	60
Figure 29: Compendium of all the yield stress points gathered from the stress sweep tests and creep tests for all the 2%, 2.5%, 3%, and 4% wt. solutions of Laponite and also shown is the equation of a fitted power law line and a exponential line corresponding to the yield stresses at a certain Laponite weight concentrations.....	61

Figure 30: This perfect circle on a Lissajous figure representing a pure Newtonian fluid.
..... 63

Figure 31: A Lissajous figure of stress and strain of a Newtonian fluid, silicone oil, at
input stress amplitudes of 3.761 Pa and 0.5919 Pa, showing that a Newtonian fluid is
characterized by a stress input and strain response that is close to a 90° phase
difference, showing a fingerprint close to a circle..... 63

Figure 32: Experimental LAOS data on the silicone oil showing the relationship between
the phase degree difference and the oscillation stress..... 64

Figure 33: Lissajous figure corresponding to a perfect elastic solid. 65

Figure 34: Lissajous figures of 2% wt. Laponite at $s = 0.5963$ and $s = 0.9454$, fit with
the model in the linear visco-elastic regime. 66

Figure 35: Lissajous figure of 2% wt. Laponite at $s = 1.5$ fit with the model as the
oscillation stress exceeds the yield stress of the solution. 67

Figure 36: Lissajous figures of 2.5% wt. Laponite at $s = 0.5$ and $s = 0.75$, fit with the
model in the linear visco-elastic regime resulting in ellipsoid Lissajous figures. 68

Figure 37: Lissajous figure of 2.5% wt. Laponite at $s = 1.2$ fit with the model as the
oscillation stress exceeds the yield stress of the 2.5% wt. Laponite solution..... 69

Figure 38: 3% wt. Laponite solution tested at $s = 0.4$ and $s = 0.7$, showing the
progression from an ellipsoid shape to a non-linear shape that deforms the ends of
the ellipsoid..... 70

Figure 39: Lissajous figure with both the experimental data and model fit for 3% wt.
Laponite as stress was increasing closer to yield stress, showing a nonlinear portion
of the fluid at $s = 0.7$ 71

Figure 40: LAOS tests of 4% wt. Laponite solution $s = 0.3$, $s = 0.5$, and $s = 0.8$ showing the transition from a linear ellipsoid to a non-linear skewed ellipsoid on a Lissajous figure of stress and strain. 72

Figure 41: LAOS data of the 4% wt. Laponite at $s = 0.8$, and fit with the same fingerprint in the model to describe the state of deformation in the fluid on a Lissajous figure of stress and strain. 73

Figure 42: Showing the transition from a linear visco-elastic ellipsoid Lissajous figure to a parallelogram nonlinear Lissajous figure of a 4% wt. Laponite solution by LAOS testing at $s = 0.5$, $s = 0.8$, and $s = 0.95$ 74

Figure 43: The comparison of Lissajous figures near the yield stress $s = 0.95$, and above the yield stress at $s = 1.1$ fit with the model for tests on the 4% wt. Laponite. 74

Figure 44: Storage modulus, G' , loss modulus, G'' , and delta plotted with respect to the oscillation stress for a 4% wt. Laponite solution to see where the yielding occurred on the solution. 75

Figure 45: Waveform showing no phase difference between the applied stress and strain response on a 4% wt. Laponite solution at $s < 1$ 76

Figure 46: Waveform of a 4% wt. Laponite solution at $s > 1$, showing the deformation and phase difference of the strain response to the applied stress. 76

List of Tables

Table 1: Error bars associated in mixing the Laponite percentage weight solutions in distilled water.....	40
Table 2: Testing parameters when using applying the stepped stress sweep tests on the Laponite solutions.....	42
Table 3: General testing parameters used when applying the creep tests on the Laponite solutions.....	43
Table 4: General testing parameters used when applying the large amplitude oscillatory tests on the Laponite solutions.....	44
Table 5: Compilation of the yield stresses determined from the stress sweep data using geometric mean from the viscosity before yielding and the viscosity after the yielding.....	50
Table 6: Compiled yield stresses extracted from the creep tests of 2%, 2.5%, 3%, and 4% wt. Laponite solutions.....	57
Table 7: Viscosity values for both the creep tests and stress sweeps tests at certain shear stresses on the 2% wt. Laponite solution.....	59
Table 8: Viscosity values for both the creep tests and stress sweeps tests at certain shear stresses on the 2.5% wt. Laponite solution.....	60
Table 9: The values used to fit the model to the experimental results of the 2% wt. Laponite LAOS tests.....	67

Table 10: Values used to fit the model to the experimental results of the 2.5% wt.	
Laponite.	69
Table 11: Values used to fit the model to the nonlinear experimental results of the 3% wt.	
Laponite at 37.65 Pa.	71
Table 12: Values used to fit the model to the experimental LAOS results of the 4% wt.	
Laponite solution.	77
Table 13: Comparing yield stress values from 2%, 2.5%, 3%, and 4% Laponite samples from the stepped stress sweeps and creep tests, with the oscillation stresses corresponding to the non-linear Lissajous figures from the LAOS tests and from the model.....	77
Table 14: Slug slime properties.	79

Chapter 1

Introduction

*The mountains flowed before the Lord, the One of Sinai, before the Lord,
the God of Israel.*

Judges 5:5

1.1 Motivation

From the bible verse above, one can infer that if even the mountains flow then one can conclude that Rheology is a study of how any material flows! Rheology is a complex subject, more exposed in higher levels of Chemical Engineering and fluids classes. Yet similar to materials research, studying basic material functions in static mechanics, it may be just as important to understand fluids characteristics when studying fluid applications. This is so that one can understand how “real” fluids might respond to stresses and strains, as any solid material would.

This undergraduate thesis was a self study on Rheology, conducted in order to gain a more in depth knowledge about the fundamentals of Rheology. From the fundamental fluid concepts learned from introductory classes, this project aims to not only extend upon that knowledge, but also to gain an understanding of how Rheology is used, and how those concepts can be applied to current research and applications. This paper will go over some of fundamental ideas concerning Rheology using basic rheological analysis

in stepped shear sweeps and creep tests, and then move onto more current research analysis using large oscillatory amplitude shear (LAOS), plotting the stress and strain responses on Lissajous figures, and matching it to a evolution of deformation model of complex fluids showing yield stress characteristics [1, 2].

1.2 Goals

The goal of this undergraduate thesis is to develop a basic understanding of Rheology through fundamental rheometer testing and analysis. Furthermore, this thesis is to learn how to use more advanced analysis using large amplitude oscillatory shear and how it can be used to characterize a fluid's material properties. By testing Laponite (material explanation in section 2) using basic rheological tests, applying LAOS tests, and then fitting it to a theoretical model, a more in-depth knowledge into Rheology can be obtained. Finally, the concepts verified by this approach will be used to emulate the properties of slug slime, leading into a further study of a mechanical slug and understanding slug locomotion.

1.3 Overview

Chapter two reviews essential background information for this project. Chapter two provides a quick broad understanding of yield stress, a little bit of its history and what current discussions there are regarding that topic. Chapter two will also discuss the material that will be extensively studied, Laponite. It will discuss its chemical structure as well as the current uses of the synthetic clay material. By mixing Laponite with water a “shake-gel” can be created. The chapter will also briefly explain the locomotion of slugs and what fluid it uses to travel.

Chapter three describes the theoretical analysis used in understanding the data extraction and explains the process in which the data is applied. It will explain the three types of testing used: stress sweep tests, creep tests, and LAOS tests, and will discuss how yield stress characteristics are extracted from the data.

Chapter four explains the procedure used to gather data, from sample preparation of the various concentrations of Laponite, to the various settings and tests used.

Chapter five shows and explains all the relevant data gathered for this experiment. It will compile and compare the various results obtained. The LAOS data will be matched and fit by the evolution of deformation model.

Finally, the conclusion will summarize the main topics discussed in this paper and the results. Further applications for Laponite and how it can be altered to be used as a medium for slug-like locomotion are discussed.

Chapter 2

Background

2.1 Yield Stress

In current rheological literature there have been numerous papers, discussions, and arguments regarding the topic of yield stress.

Yield as a general definition is used to as a term to give in or give way to. Regarding fluids, it is used the slightly different way. The definition from *An Introduction to Rheology* states that yield stress is a “stress corresponding to the transition from elastic to plastic deformation” [3]. Among the discussions, there are generally three ideas that try to define yield stress. Some say there is a gradual change in a yield “region”, some feel as if no such point exists, and others feel as if there is exactly one point where the yield occurs [4].

The three most used equations to describe yield stress liquids are the Bingham plastic model, Casson model, and the Hershel – Bulkey model[4].They are shown below:

The simplest model and probably the most well known model is the Bingham plastic model. Proposed by Professor Eugene C. Bingham, who was one of the pioneers who first defined Rheology [4].

$$\sigma = \sigma_y + \eta_p \cdot \dot{\gamma} \quad (2.1)$$

where, σ is the shear stress, σ_y is the yield stress, $\dot{\gamma}$ is the strain rate, and η_p is the plastic viscosity.

Another model is proposed by Casson which is a modification of the Bingham model,

$$\sqrt{\sigma} = \sqrt{\sigma_y} + \sqrt{\sigma_p \dot{\gamma}} \quad (2.2)$$

The Herschel – Bulkey equation is a three parameter model,

$$\sigma = \sigma_y + k \cdot \dot{\gamma}^n \quad (2.3)$$

A comparison of these three models is shown in figure 1. Although the Bingham model is the simplest it is still a good approximation of the fluid behavior of yield stress fluids.

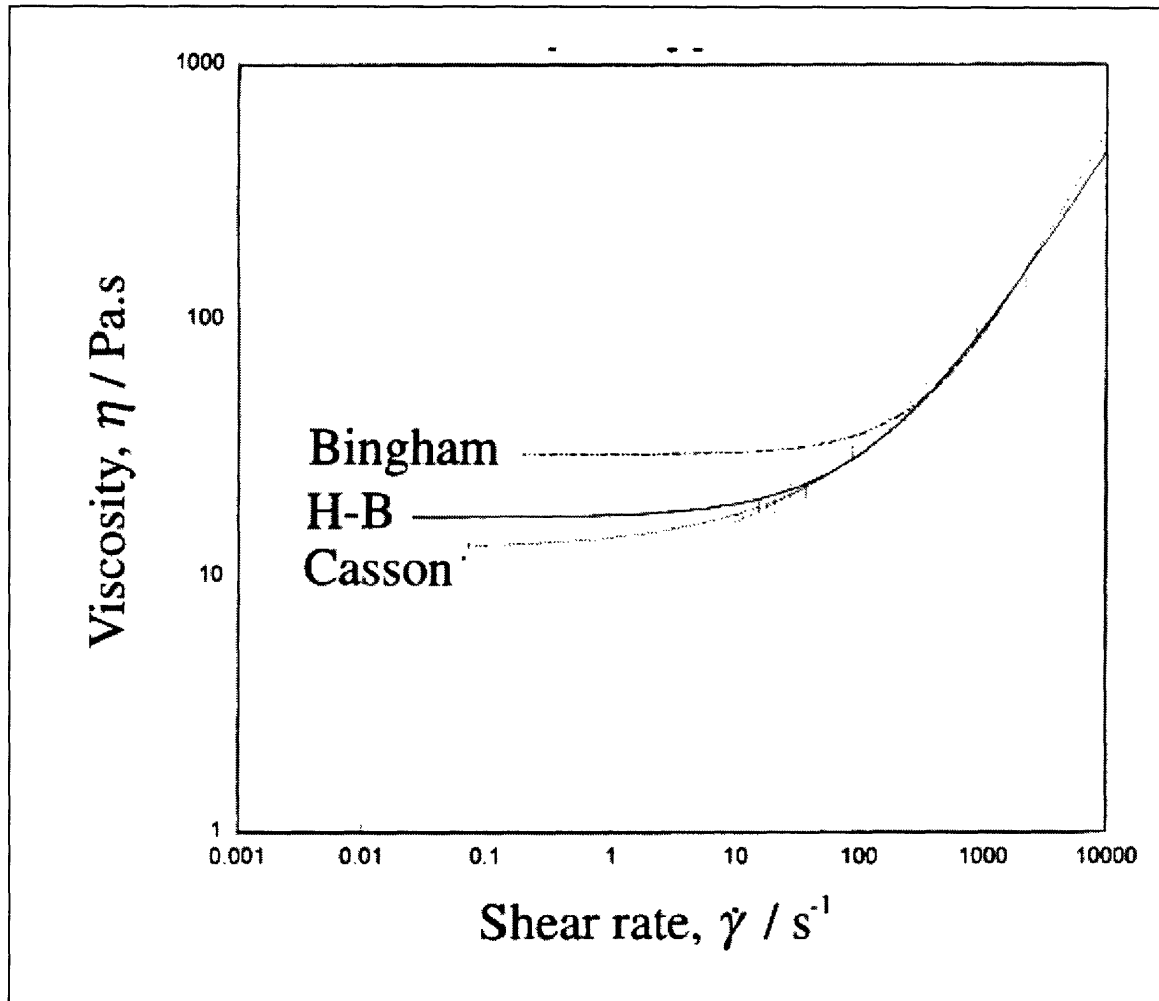


Figure 1: Compares the three most used yield stress models: Bingham, Casson, and Herschel – Burkely [4].

Other opinions, from researchers, mention yield stress as an “engineering reality,” that for practical purposes it can be used as an approximation for application [4]. There has also been discussion on the idea of an “apparent yield stress.” The concept of “apparent yield stress” is when a strict yield stress isn’t assumed to be there, when a sharp transition from a low to high viscosity fluid is present [5]. Dekee also suggests an idea of how yield stress works, that yield stress is caused by a buildup in the fluid, in which the applied stress just needs to break down in order to flow [6].

As discussed, yield stress is an important concept, but one with several differing definitions. When relating back to the engineering, as the Webster dictionary defines it, Engineering: The application of science and mathematics by which the properties of matter and the sources of energy in nature are made useful to people. It is the practical aspect of engineering that drives research towards not only academic understanding, but also useful applications that will positively impact people. Hence, being goal centric and focusing on a problem at hand, only then can a definition of yield stress be applied, not specific to the sake of science but for the sake of helping people.

2.2 Material

The material used in this study is Laponite RD from Southern Clay Products, Inc. in Gonzales, TX.

2.2.1 Structure

Laponite is a purely synthetic material, and when mixed with water it creates a type of gel, when sheared, acts as a viscous fluid. The chemical composition is $\text{Na}^{+}_{0.7}[(\text{Si}_8\text{Mg}_{5.5}\text{Li}_{0.8})\text{O}_{20}(\text{OH})_4]^{0.7}$ [7]. The particles are held together by electrostatic forces, and when Laponite is sheared, it creates a gel-like viscous fluid.

The Laponite particles are disc shaped crystals 0.92nm thick and 25nm in diameter. The electrostatic force of the particles causes the crystals to attract to the negative surfaces of the surrounding crystals, which gives the Laponite solution its gel-like formation. Stronger concentrations, lead to stronger attractive forces due to more Laponite crystals. These electrostatic forces cause the Laponite structure to be a three dimensional structure of Laponite crystals as seen in figure 2 [7].



Figure 2: A three dimensional structural form of Laponite which shows the electrostatic attraction forces on the faces and edges of the surrounding Laponite crystals [7].

Laponite is very similar to colloidal suspensions such as bentonite and hectorite in structure but is magnitudes smaller, as seen in figure 3.

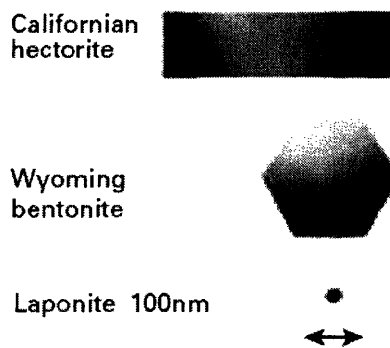


Figure 3: Shows the size magnitude difference of Laponite compared to other colloidal suspensions, bentonite and hectorite [7].

2.2.2 Current Uses

Colloid suspensions, like Laponite, are used in a variety of applications. Currently some of the fields where Laponite is used are paint, cleaning products, drilling, cosmetics, food, and pharmaceuticals [8].

Laponite is generally used where natural clays were once used [9, 10]. Laponite is chemically pure, consistent in structure, and is colorless and odorless. It is generally used as a thickening agent. When used in toothpaste, it allows the material to squeeze out of the tube, while retaining the shape when applied on the toothbrush.

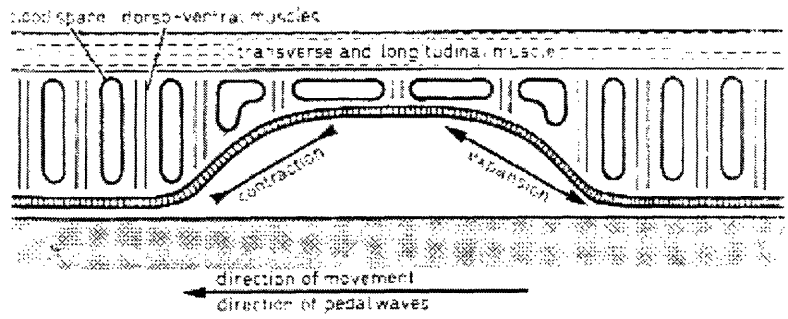
One of Laponite's more extensive uses is in the drilling industry. It is often used as a drilling fluid in heavy oil drilling machinery. As the drill bit meets the rock layer, the Laponite is used as a drilling fluid. By altering the properties of Laponite to a slurry, it is applied to where the drilling occurs to bring back up the debris.

Further uses can be applied when polymer is added onto the Laponite substance. When a polymer is added to a colloidal suspension, the additional polymer alters the rheological properties of the fluid, allowing for application specific design [8].

2.3 Slug Locomotion

Slug locomotion is an interesting phenomenon. Slugs can move over most any type of terrain, and can even climb vertically. Though slow and perhaps messy, because they leave a slime residue as they move, they have many advantageous qualities worth emulating. Research is currently being done at MIT Hatsopolous Microfluids Laboratory to understand this locomotion fully, and to emulate it with robotics, via Robosnail [11, 12].

Figure 4 shows a brief illustration of how the muscles work in order to move on a layer of slug slime. The slug moves its one foot, and from the outside observer, the layer in touch with the slime moves in a wave-like pattern down the length of the snail, slowly moving across the terrain, and leaving behind a layer of slime.



[<http://www.arnobrosi.com/slugbio.html>]

Figure 4: Illustration of how a slug contracts and expands its muscles in order to use the slug slime as a means of locomotion.

A rough analysis of the fluid is done below for a slug climbing vertically on a wall (figure 5).

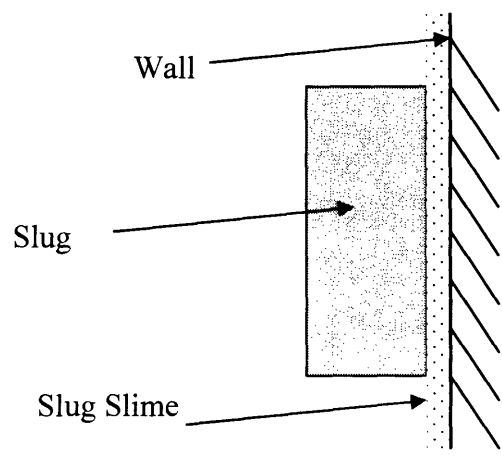


Figure 5: Rough diagram of a slug fixed onto a vertical wall on a layer of slug slime.

In figure 5, a slug is stuck onto its own slime and resting on the wall. The dimensions of the slug are

$$WxDxH = V \quad (2.4)$$

where W is the width, D is the depth, H is the height, and V is the approximated volume. Its density is given by ρ , and the force, F , that's acting on the slime face due to gravity, g , is

$$F = mg = (\rho \cdot V) \cdot g \quad (2.5)$$

The shear stress, τ , that the force is causing on that face is given by

$$\tau = \frac{F}{HW} = \frac{(\rho \cdot V) \cdot g}{HW} \quad (2.6)$$

which has units of pressure.

Using the Bingham plastic model to model the slug slime, the object will start falling if

$$\tau = \sigma_y \quad (2.7)$$

σ_y being the yield stress of the slug slime.

After substituting and rearranging,

$$\sigma_y = \frac{\rho V g}{HW} \text{ and } V = WDH, \quad (2.8)$$

then one can conclude that if

$$\sigma_y > \rho Dg \quad (2.9)$$

Looking at banana slugs, the second largest among the slug family, and doing an order of magnitude estimate, the weight is about 0.2 kg [13, 14], length is about 20cm [15], and its

width is approximated to about 5 cm. By this estimation, that σ_y has be greater than 200 Pa!

As the yield stress is very high on the fluid, it is understandable how it manages to stay attached to the wall, but it is phenomenal to see that slugs' ability to not only stay, but to travel along vertical walls.

At this point, an application to the slug slime will be constructed using the analysis and rheological characterization done on the Laponite fluid, coupled with the understanding of these properties of slug slime.

Chapter Three

Theoretical Analysis

3.1 Stress Sweep and Observing Yield Stress

A shear stress can be applied in a step-wise manner from a low stress to a high stress. After a certain region or point, the material transitions from a solid-elastic material, to a viscous fluid. By applying a stress sweep, one can observe a change in the viscosity as a function of the stress. After a yield stress material has been sheared from a low shear stress to a high stress, and then sheared in the opposite direction from a high stress to a low stress, hysteresis can be observed, similar to that of solid elastic theory.

Elastic solid theory, as shown in figure 6, shows that when an elastic material is applied a shear stress, the value of the strain goes linearly upwards corresponding to the Young's modulus. When the stress exceeds the yield stress, the material starts to strain harden, and when unloaded, unloads corresponding to the Young's modulus and back into its original form.

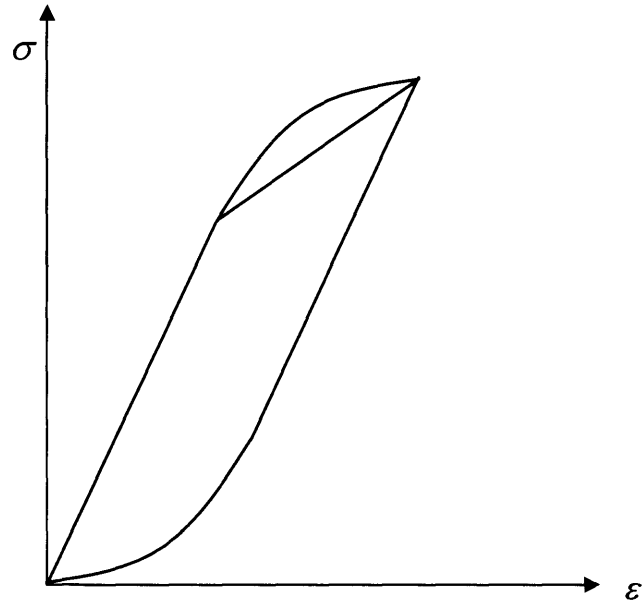


Figure 6: Theoretical hysteresis loop for a metal plotted on stress and strain axes.

Similarly as an elastic solid, when applying a stress to a yield stress fluid it can be modeled the same way. The fluid loads according to a modulus then becomes a viscous fluid after the yield stress. When unloaded, it slowly comes back to its original form. This phenomenon is seen in figure 7 and is verified in section 3.3.

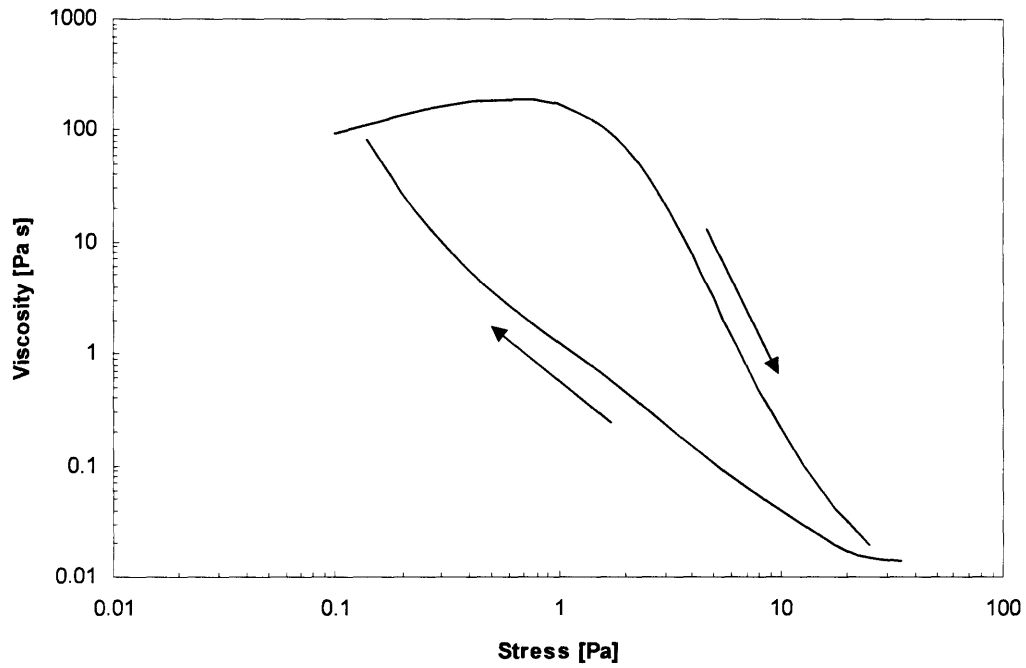


Figure 7: Hysteresis curve of a sample fluid as the stress is swept up and down.

From the graph in figure 7, using a geometric mean from the high viscosity value and the low viscosity value, that value scaled down to the respective stress can be categorized as the yield stress.

$$\eta_y = \sqrt{\eta_H \cdot \eta_L} \quad (3.1)$$

where, η_y is the viscosity at yield stress, η_L is the viscosity when yielded, and η_H is the viscosity before the fluid gets to the yield point.

3.2 Creep and Observing Yield Stress

When a material undergoes creep testing, it is tested at one stress value and the deformation is shown over time. It deforms the fluid and measures the strain with respect to the length of time the stress is applied. In different ratios of input stress to yield stress ($s = \sigma_o / \sigma_y$) different fluid strain responses are seen in figure 8.

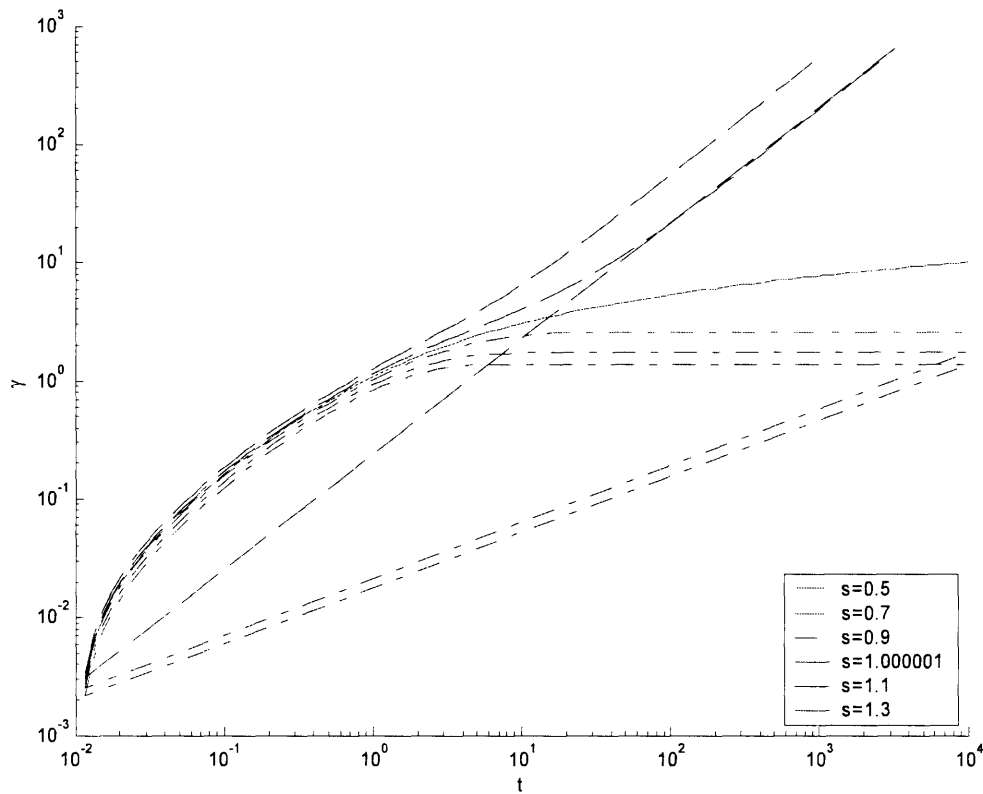


Figure 8: Matlab graph illustrating the effect of $s = \sigma_o / \sigma_y$ on creep tests.

Values under a ratio of $s < 1$, the material strain approaches a constant value. As the ratio of input stress to yield stress exceeds 1, the strain values increase linearly with time on a log scale. Citerne [16] used the creep graphs to see a visible difference between the results of $s < 1$ and $s > 1$ corresponding to visible difference in an elastic response and a

viscous response. By using observing those visible differences a yield stress can be determined from the transition from the elastic response to the viscous response. This same analysis can be used in this case to approximate the yield stress and match it with the yield stress values obtained in the shear stress analysis.

By doing creep tests on yield stress values obtained from the stress sweeps, a range of effects can be seen with respect to various input stresses. By applying a stress in which exhibits high viscosity, the strain levels out at a low value, and by applying a stress which exhibits low viscosity, the material linearly deforms on a log-log plot. By applying a creep test with $s = 1$, as determined on the stress sweep, and marginally increasing and decreasing that value for use in creep tests, one can see where the transition from an elastic-solid to a viscous liquid occurs. These tests can verify the yield stress value obtained in the stress sweep tests.

By plotting the strain graphs as compliance, the opposite of a modulus, one can also get a better look at the viscosity analysis. How the viscosity values are extracted from a compliance graph is shown in the simple analysis below.

Stress by definition is:

$$\sigma = \eta \cdot \dot{\gamma} \quad (3.2)$$

where σ is the stress, η is the viscosity, and $\dot{\gamma}$ is the strain rate.

This can also be shown as:

$$\sigma = \eta \cdot \frac{d\gamma}{dt} \quad (3.3)$$

where γ is the strain, and t is time.

Integrating with the initial condition that at $t = 0, \gamma = 0$, and rearranging,

$$\gamma = \frac{\sigma}{\eta} \cdot t \quad (3.4)$$

Compliance is defined as strain over stress, finally giving the relationship.

$$J = \frac{\gamma}{\sigma} = \frac{t}{\eta} \quad (3.5)$$

where J is the compliance.

Using this relationship, one can fit the viscosity values from the compliance graphs onto a stress sweep graph to verify the obtained results.

By comparing the yield stress from the stress sweeps with an estimated one from the creep experiments and fitting the viscosity values from the compliance graphs, one can see if the two tests are comparable.

3.3 Large Amplitude Oscillatory Shear and Observing Yield Stress

By applying the equations [1, 2] the coupled nonlinear equations below describe the state of deformation in a fluid showing yield stress properties.

When an oscillatory shear stress is applied a strain rate can be modeled as:

$$\dot{\gamma} = \frac{1}{\tau \cdot G} [\sigma_o \cdot \cos(\omega t) - G \cdot \Delta(t)] \quad (3.6)$$

where $\dot{\gamma}$ is the strain rate, τ is the time constant, G is the modulus, σ_o is the input stress, ω is the frequency, t is the time, and $\Delta(t)$ is the population imbalance of defects in the material.

The rate of change of the population imbalance of defects in the material is given by:

$$\dot{\Delta} = \dot{\gamma} \left[1 - \frac{G \cdot \sigma_o \cdot \cos(\omega t)}{\sigma_y^2} \Delta(t) \right] \quad (3.7)$$

where σ_y is the yield stress.

When the coupled non-linear ordinary differential equations are solved for materials fitted with a proper modulus, time constant, frequency, input stress, and yield stress, solutions can then be applied on a Lissajous figure of stress and strain. This would show a rheological “fingerprint” illustrating the characteristics of the material at certain parameters. For instance as a function of input stress to yield stress, $s = \sigma_o / \sigma_y$, various different “fingerprints” can be examined. When $s = \sigma_o / \sigma_y < 1$, the linear elastic response is shown, resembling a straight elliptical shape in the Lissajous figure. As $s = \sigma_o / \sigma_y$ approaches 1, the non-linearities are introduced into the Lissajous figure and it becomes bigger with the edges becoming more skewed. As $s = \sigma_o / \sigma_y$ exceeds 1, the Lissajous figure becomes a parallelogram, showing the accumulated deformation and strain in the Lissajous figure. The various Lissajous figures corresponding to different input stress to yield stress ratios are seen in figure 9.

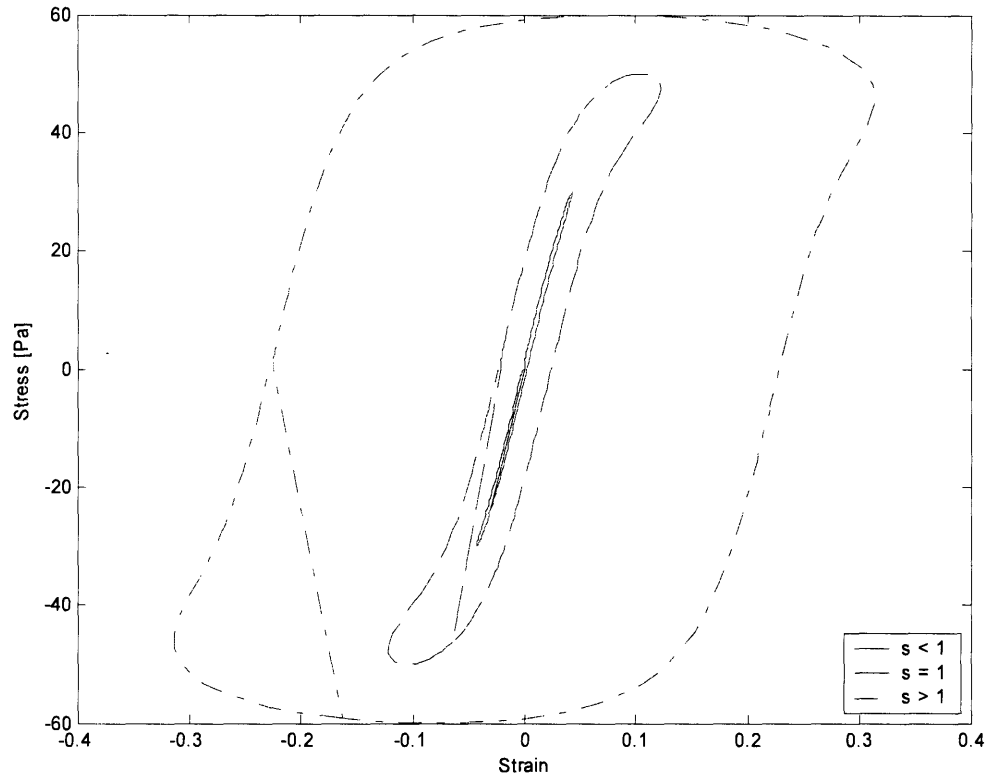


Figure 9: Compares the Lissajous figures of $s = \sigma_o/\sigma_y < 1$, $s = \sigma_o/\sigma_y = 1$, and $s = \sigma_o/\sigma_y > 1$ using the evolution of deformation model.

By using large amplitude oscillatory shear, the Lissajous figures can be used to further verify the yield stress values from the stress sweep tests and creep tests, by exhibiting specific shapes corresponding to the values from the stress sweep and creep tests.

Chapter Four

Experimental Methods

The experiments performed were three different types of tests to characterize the concentrations Laponite gels: stepped stress sweeps, creep tests, and large amplitude oscillatory tests. All tests were performed on an AR1000 rheometer, seen in figure 10, with a 40mm, 1.59 degree cone and plate geometry all at 20° C.

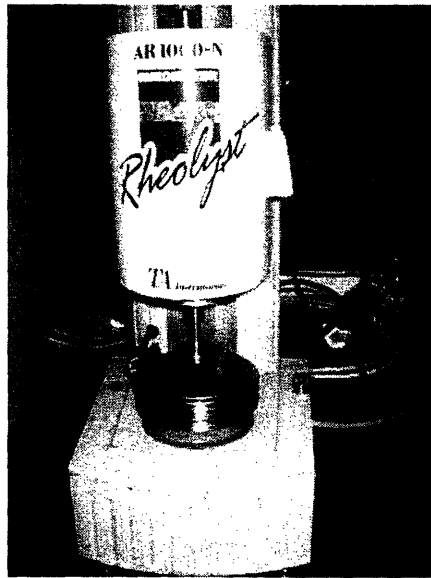


Figure 10: AR1000 used for all the stress sweep, creep, and large amplitude oscillatory shear tests on the Laponite solutions.

4.1 Sample Preparation

Samples were prepared by mixing Laponite with distilled water. The weight percentages that were prepared were 1%, 2%, 2.5%, 3%, and 4% wt. solutions. The mixture was prepared at room temperature into 100 mL solutions, and then mixed for 72 hours to ensure complete mixture. Then, the solutions then sat at room temperature for 3 days to make sure the Laponite mixture settled and the beginning aging effects would not affect the results significantly [17].

The fully mixed solutions were carefully placed on a scale. The Laponite was measured to 0.001g accuracy and the distilled water was measured to 0.01g accuracy.

The error bars are noted in the table below.

Table 1: Error bars associated in mixing the Laponite percentage weight solutions in distilled water.

Concentration	Error Bars
1%	± 0.1005
2%	± 0.0412
2.5%	± 0.0412
3%	± 0.0348
4%	± 0.0264

The 2%, 2.5%, 3%, and 4% Laponite distilled water mixtures that were made a type of gel material. The solutions when left out undisturbed would feel like a gel type material. When shaken, the solution would then flow like a viscous fluid. Figures 12-13, show a graphic illustration of the Laponite mixture states, before being shaken and after being shaken.



Figure 11: A sample of 3% wt. Laponite solution upside down before being shaken, the stir bar suspended in the gel shows the elastic gel-like properties.



Figure 12: A sample of 3% wt. Laponite solution, upside down after being shaken, showing the viscous fluid-like properties.

4.2 Stress Sweep

By applying a stepped stress sweep on each of the concentrations, a relationship of stress to viscosity was shown. The experimental parameters are shown in table 2 below.

Table 2: Testing parameters when using applying the stepped stress sweep tests on the Laponite solutions.

Conditioning Step:			
Initial Temperature		Pre-Shear	Equilibrium
20 C		10 seconds	10 seconds
Steady Step Flow Step:			
Stress Range [Pa]	Points a Decade	Temperature	Sample Period
5.968 E-3 ~ 5968	5	20 C	20 seconds
Steady State:			
Percentage Tolerance		Consecutive within Tolerance	Max. point time
5%		3	1 minute

The observations during testing show that the sample does not reach the equilibrium stated in the range specified by the 5% tolerance, but it would at least stay within the 10% tolerance range.

The stress sweep tests were stepped up from 0.005968 Pa to 5968 Pa. On the step up procedure, the test would finish when the rheometer would overspeed. Once the procedure was complete, on the same sample, the stress would then be stepped back down from the last point 0.005968 Pa. The rheometer would then stop gathering data at the point where the change was too small for the resolution of the rheometer to pick up. This shear step up and down procedure made the hysteresis in the fluid visible.

The main goal was to understand the yield stress of the material at certain concentrations. Creep tests would directly follow the stress sweep tests to verify the data received.

4.3 Creep

By applying a creep test we were able to see at certain stresses how the strain would change over time. Testing was done at various stresses, ranging from the solid-like regime to the liquid-like regime in order to see the stark contrast between the two. By observing the results in the stress sweeps, values were chosen for the solid regime, and the viscous regime, depending on the high and low viscosities the shear stresses would correlate to. For each fluid, thorough testing was performed to verify the yield stress results for the stress sweep step tests, by testing points to see clearly what the yield stress might be. The testing parameters are shown below.

Table 3: General testing parameters used when applying the creep tests on the Laponite solutions.

Conditioning Step:		
Initial Temperature	Pre-Shear	Equilibrium
20 C	10 seconds	10 seconds
Retardation:		
Temperature	Equilibrium Time	Points a Decade
20 C	2 minutes	5
Steady State:		
Percentage Tolerance	Consecutive within Tolerance	Sample Period
5%	3	20 seconds

4.4 Large Amplitude Oscillatory Shear

For each Laponite concentration an oscillatory shear was applied. For a stepped oscillation stress input a strain response was obtained. The tests were performed at 0.1 Hz, pre-sheared, and at a sampling cycle of 5 cycles. Once obtained, the data was then compared to the visco-elasto-plastic model in section 3.3. The stress oscillation gave an overview of the points and showed how it compared to the stress sweep results. A strain sweep was also done in order to get more data close to where the ratio of input stress approached the yield stress. An AR2000 was used for the strain sweep tests since the AR2000 has a better resolution than the AR1000.

Table 4: General testing parameters used when applying the large amplitude oscillatory tests on the Laponite solutions.

Conditioning Step:				
Initial Temperature		Pre-Shear	Equilibrium	
20 C		10 seconds	10 seconds	
Steady Sweep Step:				
Sweep [micro N m]	Points a Decade	Temperature	Equilibrium Time	Frequency [Hz]
0.10 ~ 1.00E5	5	20 C	1 minute	0.1
Steady State:				
Percentage Tolerance		Consecutive within Tolerance	Max. Point Time	
5%		3	1 minute	

Chapter 5

Results and Discussions

5.1 Stress Sweep

Using the stepped stress sweep methods described in section 4, tests were applied to 1%, 2%, 2.5%, 3%, and 4% wt. solutions of Laponite.

Figure 13 shows the stepped stress sweep data for the 1% wt Laponite solution. It shows that it is very similar to that of a Newtonian liquid. It is evident it does not show a yield stress, or a characteristic that at a certain stresses there is a difference in how the material flows. The comparison to a Newtonian fluid can be seen in figure 14. The plot in figure 14 shows silicone oil tested at the same testing procedure as the 1% wt. Laponite. It shows a low viscosity and a constant viscosity value throughout the entire stepped stress sweep. Understanding there are no interesting characteristics for the 1% wt. solution, no further testing was applied to that sample.

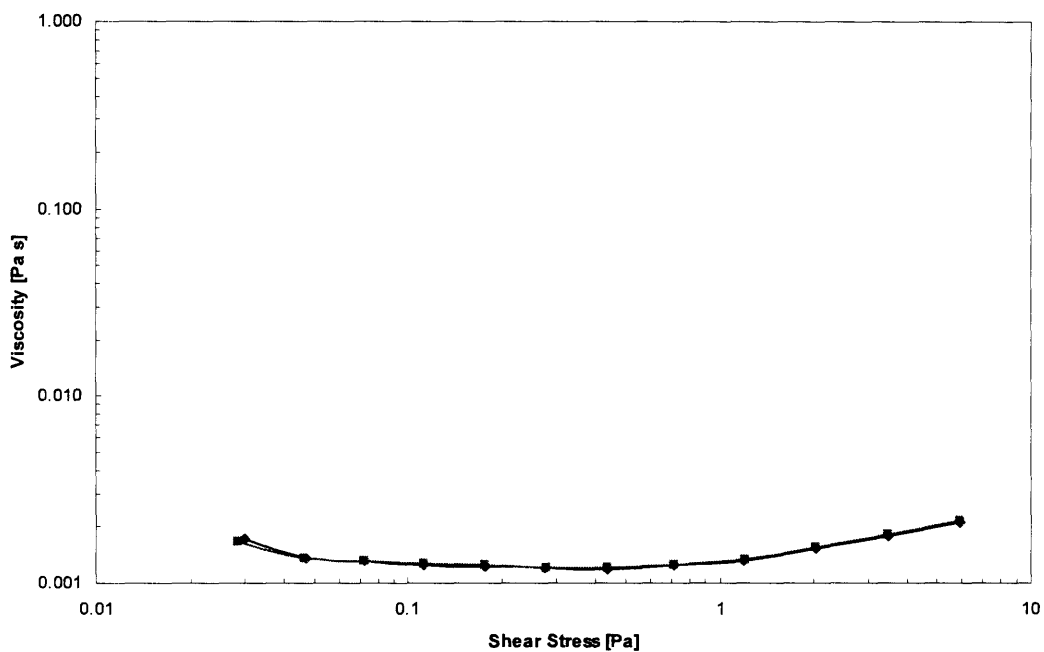


Figure 13: Two tests of stepped stress sweeps of a 1% wt. Laponite-water solution, showing no yield stress characteristics.

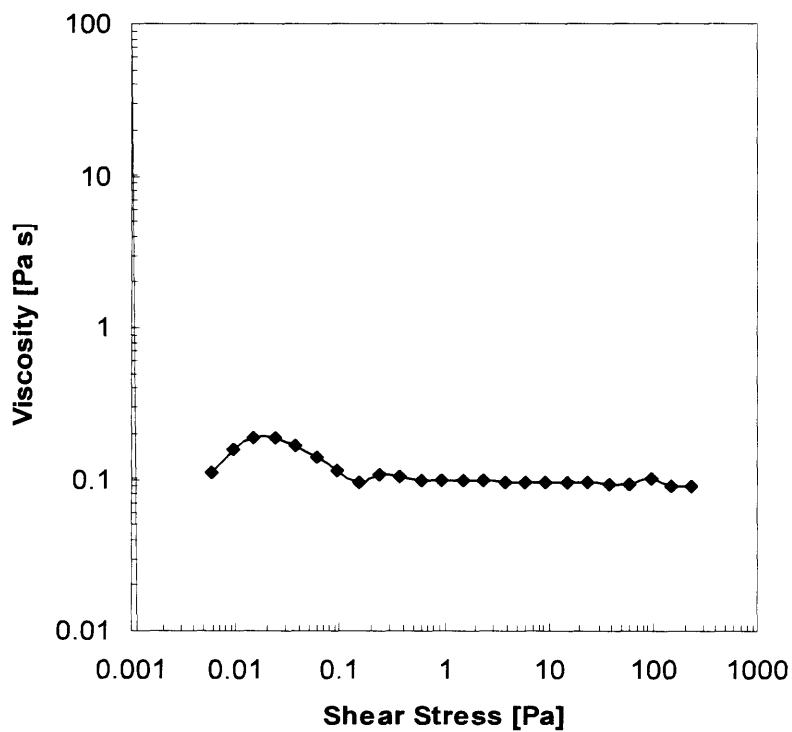


Figure 14: Stress sweep test of silicone oil that showing characteristics of a Newtonian fluid.

Figure 15 shows a 2% wt. concentration of the Laponite water mixture. This solution shows very different characteristics than that of the 1% wt. concentration. Through a stepped stress sweep up and down, a hysteresis can be shown as mentioned in section 4.1. In the region of 1Pa to 10Pa, there is a slow drop in viscosity, corresponding to the fluid yielding in that region.

By applying a simple geometric mean, using equation 3.1, of the viscosity before yielding and viscosity after yielding, the corresponding yield stress is 4 Pa.

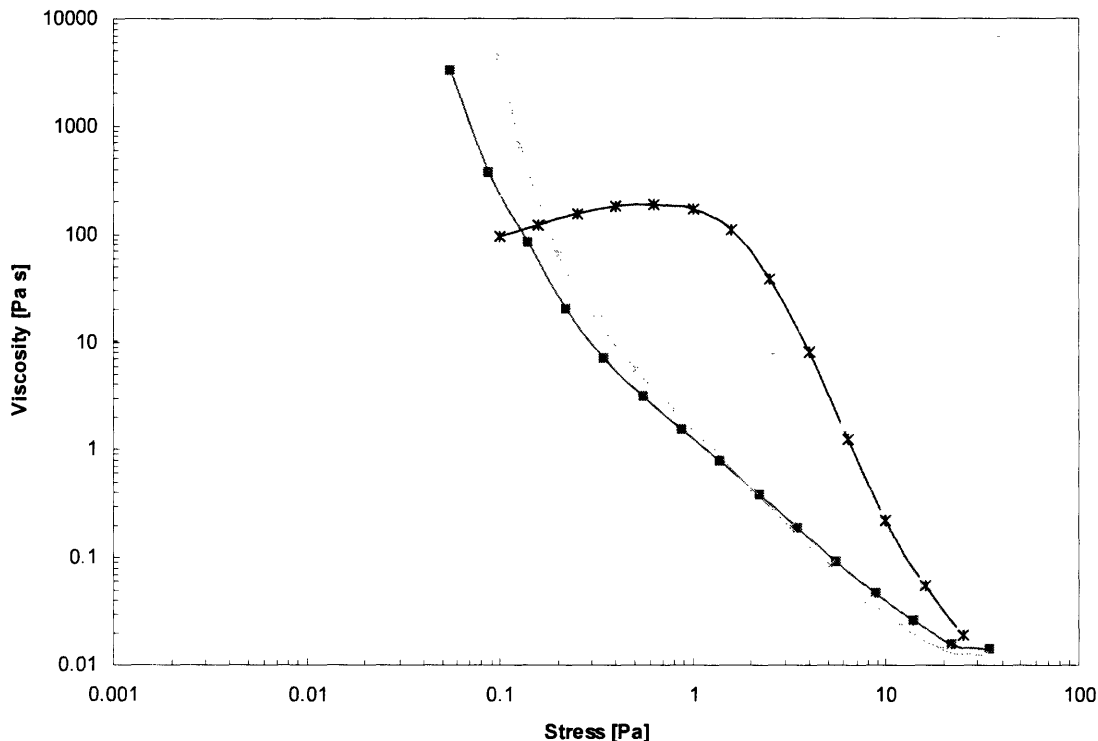


Figure 15: Numerous stress sweep tests stepped up and down on 2% wt. concentration of Laponite and water, showing yield stress characteristics and a hysteresis.

The 2.5% wt. concentration of Laponite in figure 16 shows a steeper decrease in viscosity than shown in the 2% wt sample. This demonstrates a more defined yield stress as opposed to a region of yielding in the 2% wt. concentration in figure 2.

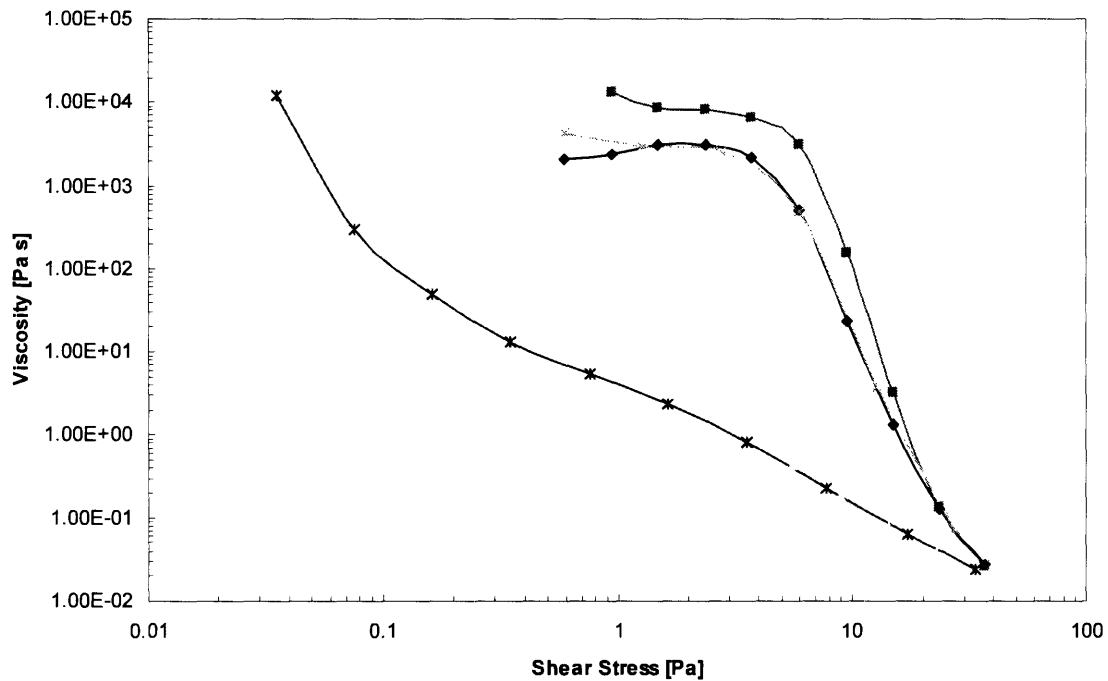


Figure 16: Numerous stress sweep tests stepped up and down on 2.5% wt. concentration of Laponite and water, showing yield stress characteristics and a hysteresis.

The following figures 17-18 show that the 3% wt. concentration and the 4% concentrations have an even steeper drop in viscosity after a certain yield stress or point. Another observation shows that the hysteresis the reverse stress sweep goes back to the original viscosity much more quickly in the higher concentrations than the lower concentrations, showing a faster restructuring time than the lower concentrations.

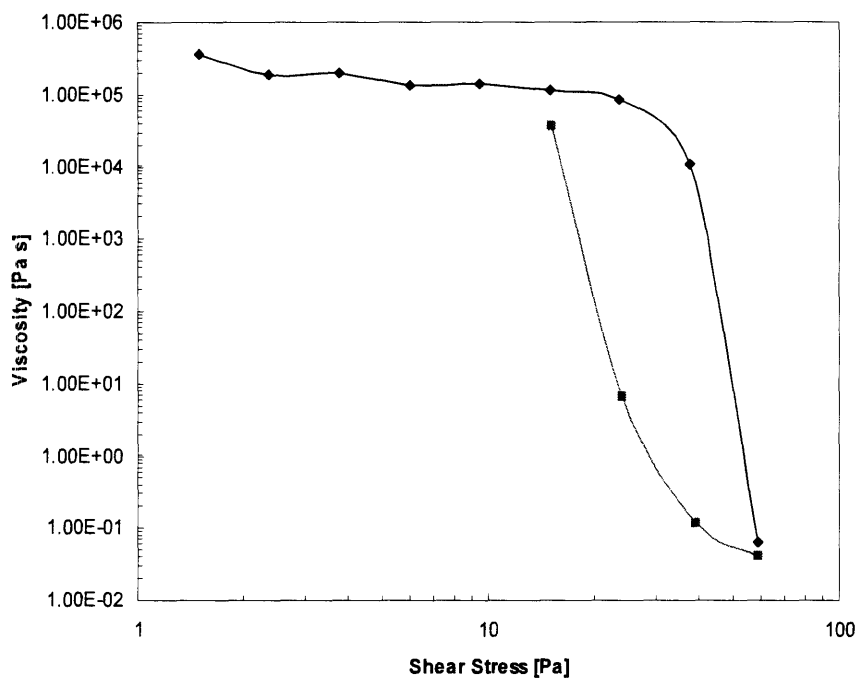


Figure 17: Numerous stress sweep tests stepped up and down on 3% wt. concentration of Laponite and water, showing yield stress characteristics and a hysteresis.

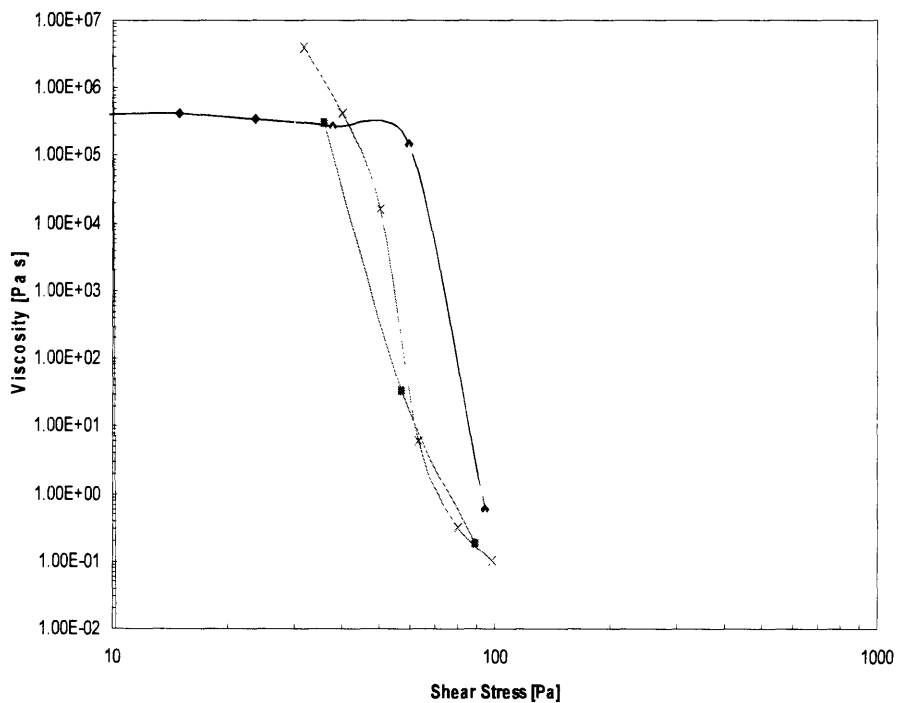


Figure 18: Numerous stress sweep tests stepped up and down on 4% wt. concentration of Laponite and water, showing yield stress characteristics and a hysteresis.

By combining the above stepped stress sweep graphs, a clear difference can be seen in the various concentrations. In figure 13, the 1% wt. Laponite solution shows no yield stress. The 2%, 2.5%, 3%, and 4% wt. Laponite all show clear signs of yield stress. The only exception might be the 2% wt. Laponite solution, it is a very gradual perhaps showing a yield stress region. By applying the geometric mean, table 5 shows the yield stresses correlating with the stress sweep tests.

Table 5: Compilation of the yield stresses determined from the stress sweep data using geometric mean from the viscosity before yielding and the viscosity after the yielding.

Concentration	Yield Stress
1%	none
2%	4 Pa
2.5%	11 Pa
3%	52 Pa
4%	75 Pa

On a log-log scale it looks as if the viscosity is decreasing drastically when the shear stress is above the yield stress. Though, when looking at the graphs on a semi-log scale, one can observe that the viscosity of all the samples drops in about an absolute 20 Pa range. Figures 19-21 show the stress sweep data for the 2%, 3%, and 4% solutions on a semi-log scale.

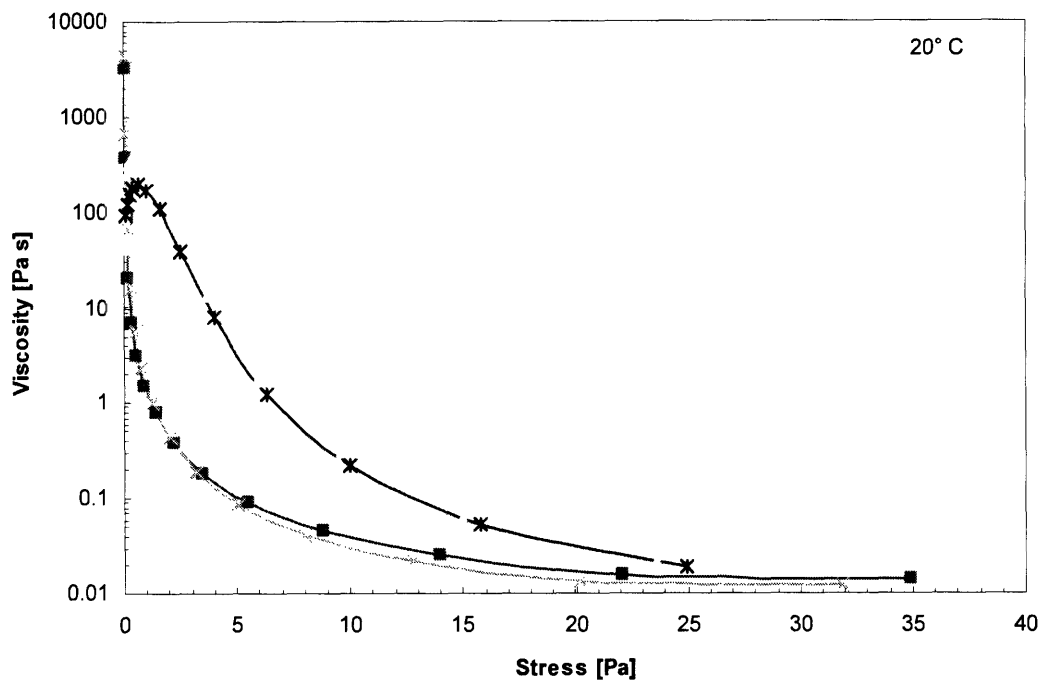


Figure 19: Semi-log scale of the 2% Laponite solution when applied a stepped stress sweep test.

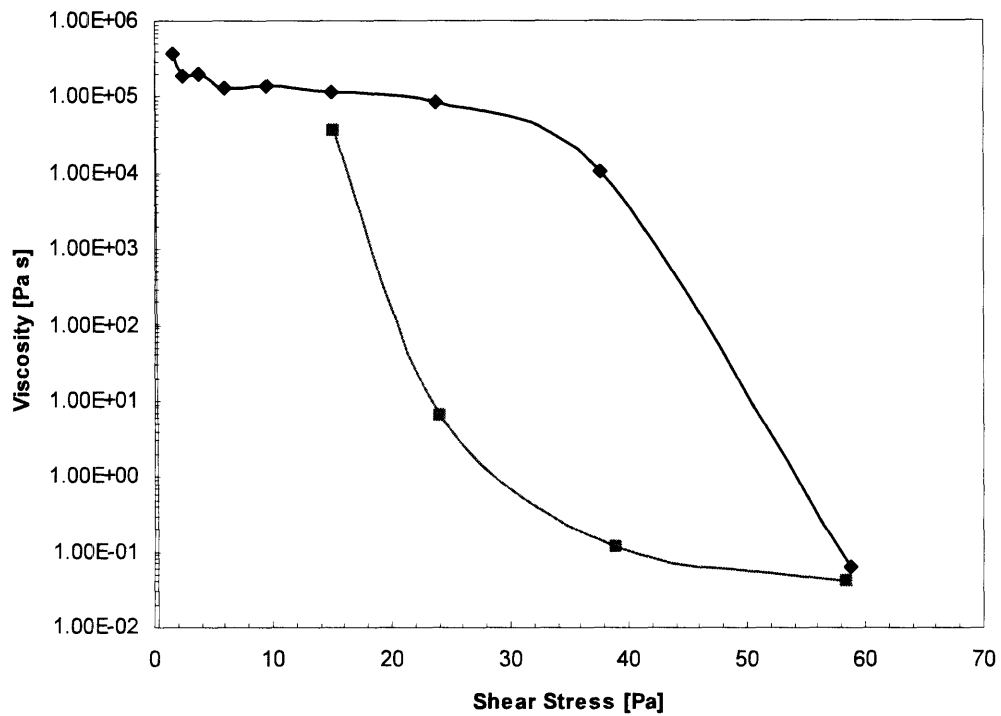


Figure 20: Semi-log scale of the 3% Laponite solution when applied a stepped stress sweep test.

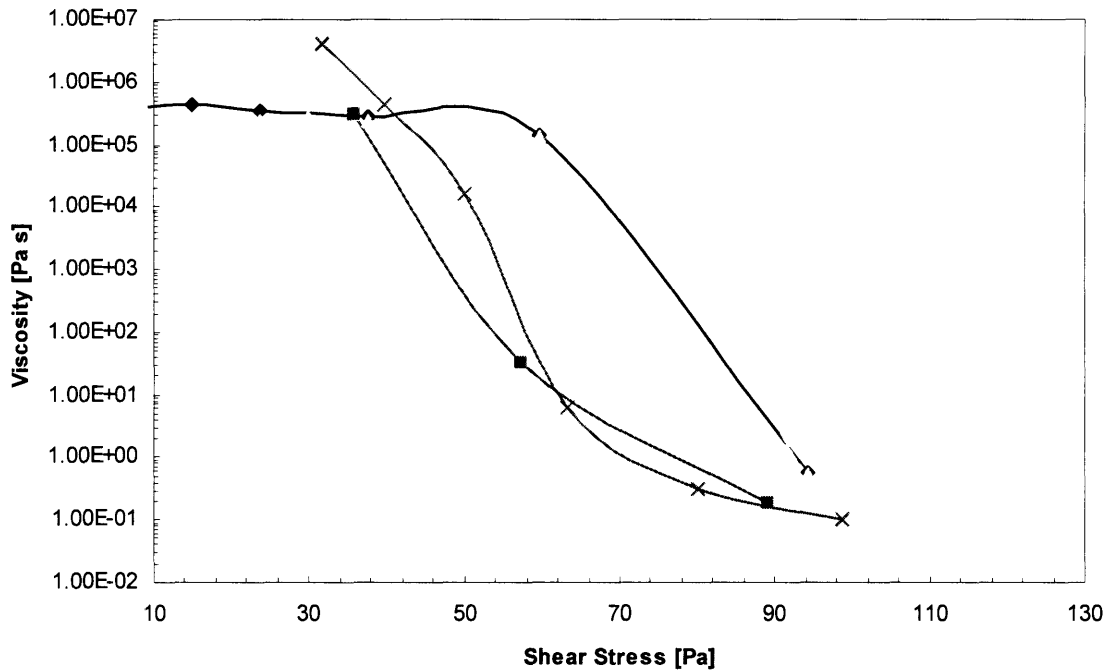


Figure 21: Semi-log scale of the 4% Laponite solution when applied a stepped stress sweep test.

Though it may seem that with each increase in Laponite concentration, there is a steeper drop in viscosity, the drop in viscosity is mainly done in a 20 Pa window in the fluid. In figure 22, plots of all the stepped stress sweep tests are combined onto one graph. It shows the difference in how each concentration mixture is affected by the varying shear stresses. An increase concentration of Laponite corresponds to higher yield stress values.

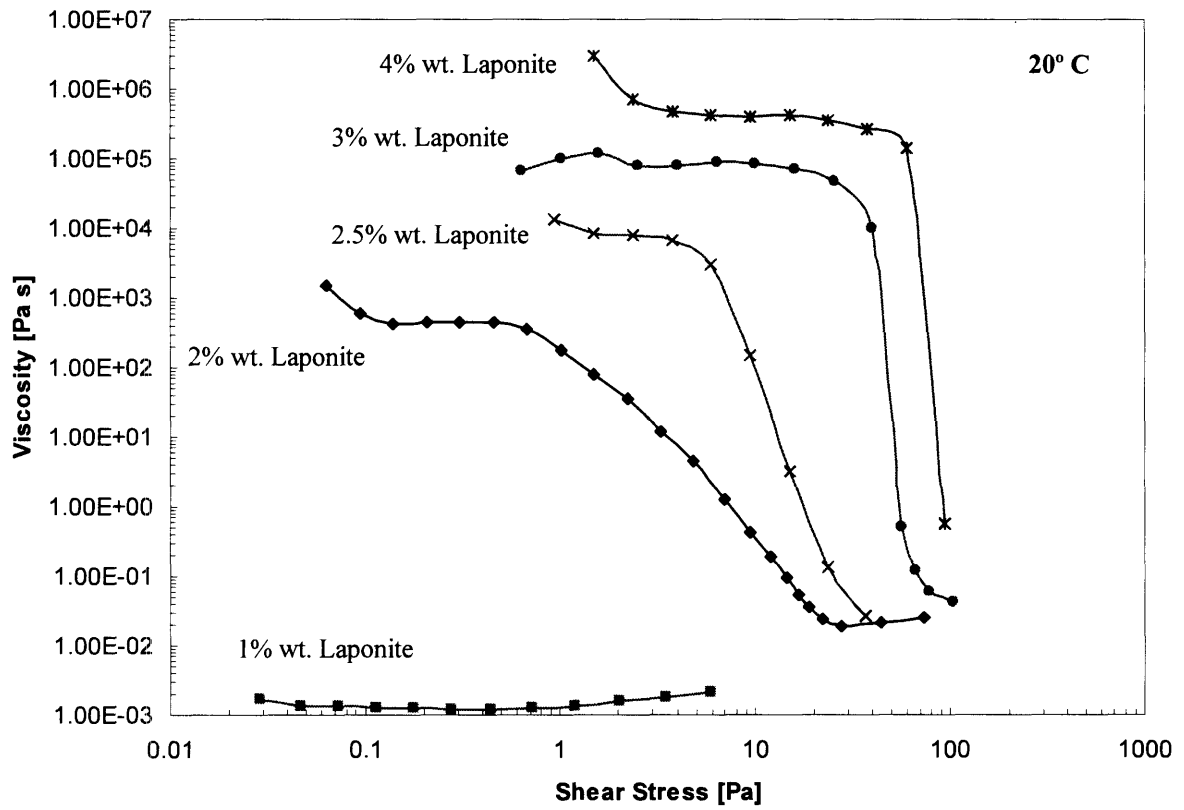


Figure 22: Compendium of the stepped stress sweep curves for the 1%, 2%, 2.5%, 3% and 4% wt. Laponite solutions all at 20°C.

5.2 Creep

Creep testing was conducted to verify the stepped stress sweep tests. For 2% wt. Laponite, the yield stress according to the stress sweeps were determined to be around 4 Pa. In the creep tests shown in Figure 23, one can see that there is a big difference between the 6 Pa test and the 9 Pa tests, while the 15 Pa test and 9 Pa test behaved similarly. For such a big difference in stress values and to behave similarly, and for such a small difference in values to behave so differently shows that the yield stress must be around the 6 Pa mark. This evidence can also be seen in the difference of the 6 Pa creep test and the 3 Pa creep test. Since there is a drastic difference in the way the fluid flows, one can assume that there be a corresponding yield stress in that region of shear stress values.

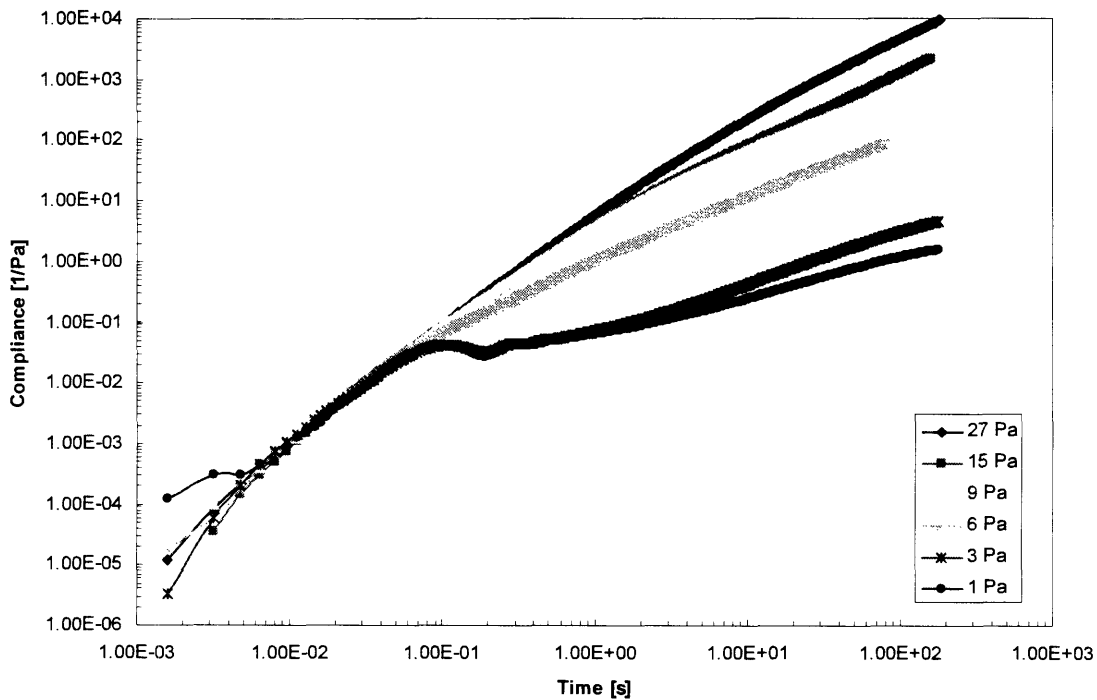


Figure 23: A comparison of the Compliance $J(t)$ for the creep tests on a 2% wt. solution of Laponite when applied shear stresses from 1 Pa to 27 Pa, showing the difference in creep tests done with shear stresses below the yield stress and shear stresses above the yield stress value.

By applying the same analysis for the 2% wt. Laponite solution in figure 23, yield stresses can be estimate in the creep graphs in figures 24-26 for the 2.5%, 3%, and 4% wt. Laponite data.

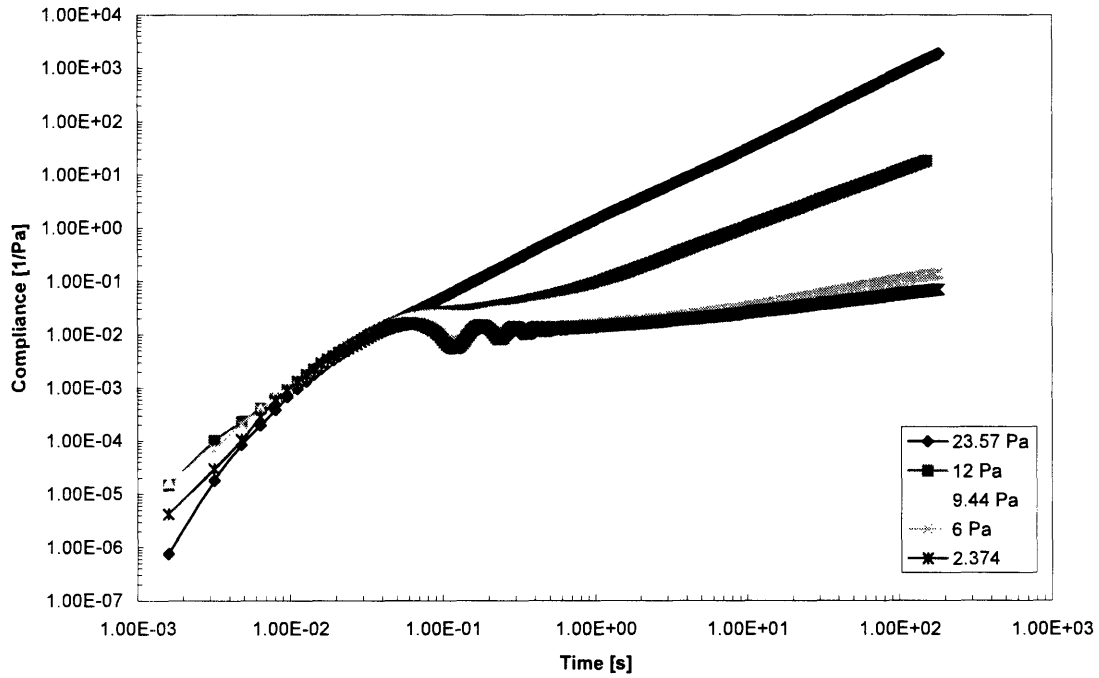


Figure 24: A comparison of the Compliance $J(t)$ for the creep tests on a 2.5% wt. solution of Laponite when applied shear stresses from 2.374 Pa to 23.57 Pa, showing the difference in creep tests with shear stresses below the yield stress value and shear stresses above the yield stress value.

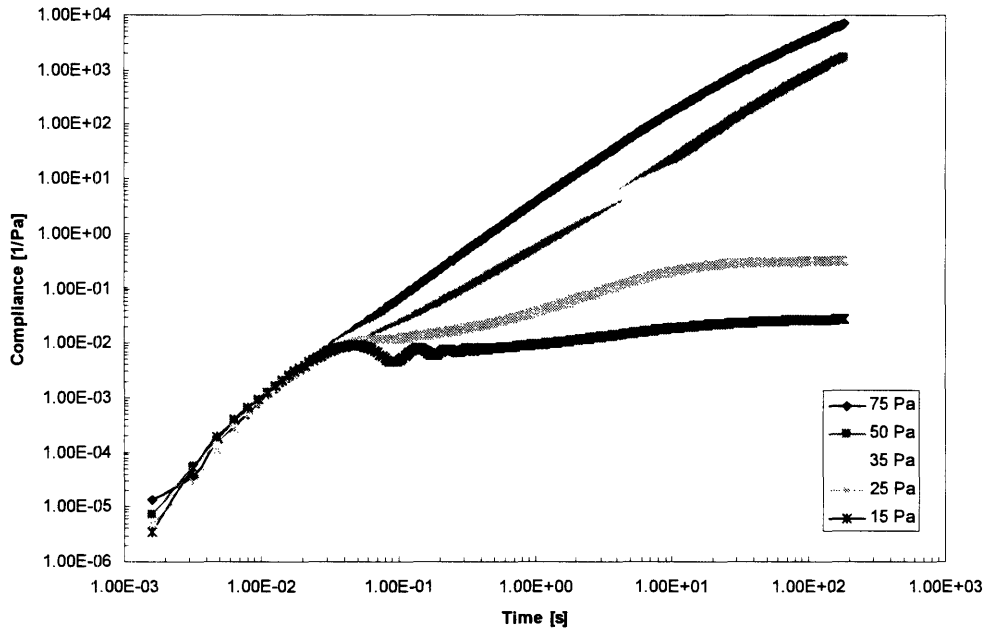


Figure 25: A comparison of the Compliance $J(t)$ for the creep tests on a 3% wt. solution of Laponite when applied shear stresses from 15 Pa to 75 Pa, showing the difference in creep tests with shear stresses below the yield stress value and shear stresses above the yield stress value.

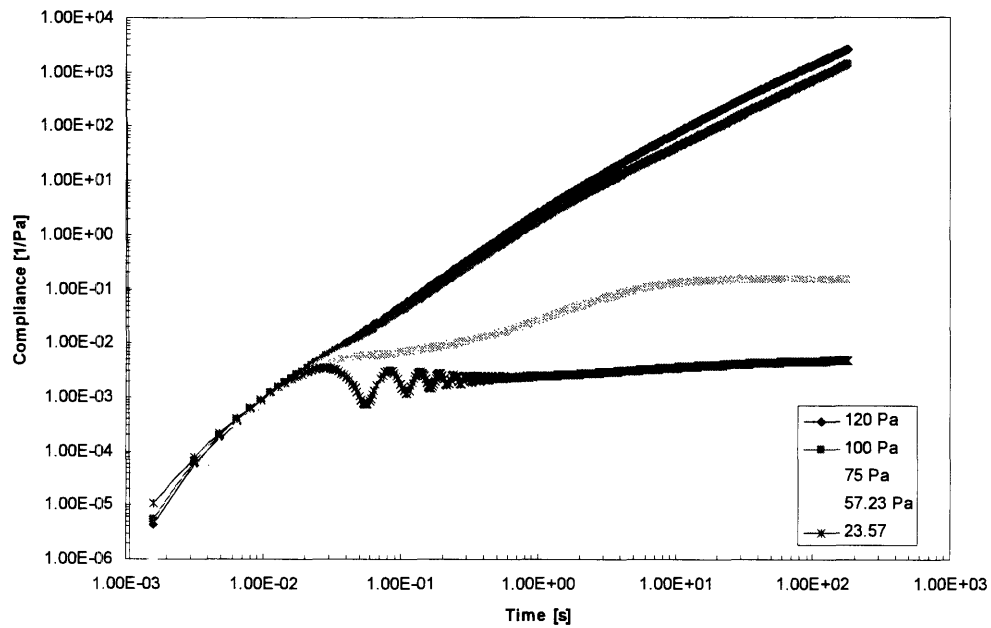


Figure 26: A comparison of the Compliance $J(t)$ for the creep tests on a 2.5% wt. solution of Laponite when applied shear stresses from 23.57 Pa to 120 Pa, showing the difference in creep tests with shear stresses below the yield stress value and shear stresses above the yield stress value.

Compiling all the data gathered from the creep tests, table 6 shows the yield stresses obtained from the creep analysis.

Table 6: Compiled yield stresses extracted from the creep tests of 2%, 2.5%, 3%, and 4% wt. Laponite solutions.

Concentrations	Yield Stress
2%	5 Pa
2.5%	12 Pa
3%	32 Pa
4%	90 Pa

Now using any one of these graphs, one can also verify the viscosity results of the stress sweep tests by using the analysis in section 3.3. Using the Compliance graph of 2% wt. Laponite in figure 22 , the viscosity values can be extracted from the graph and fitted right onto figure 15, the stepped stress sweep plot of 2% wt. Laponite. One can see that the overlap in figure 27 is reasonable. This allows the reassurance that the two test results are similar with also similar yield stresses.

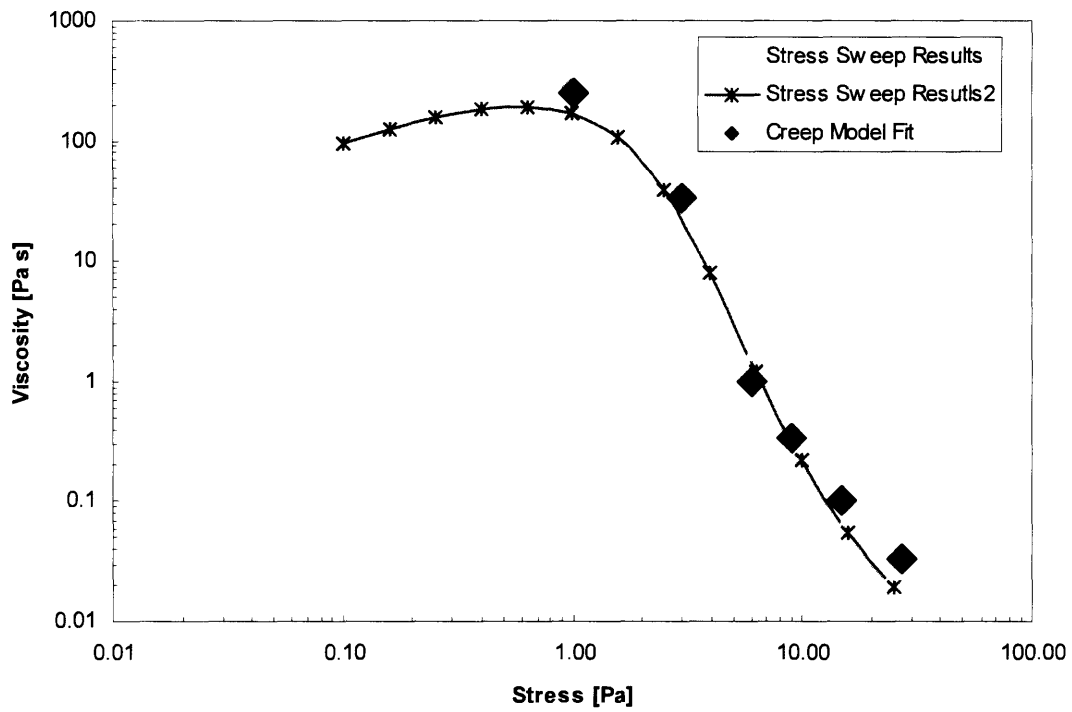


Figure 27: A fit of the creep test extracted viscosity values for a 2% wt. Laponite solution mapped onto the stepped stress sweep data for the same 2% wt. Laponite sample.

Table 7, shows the comparison of the stress sweep test viscosity values to the creep test viscosity values to evaluate how closely the values line up.

Table 7: Viscosity values for both the creep tests and stress sweeps tests at certain shear stresses on the 2% wt. Laponite solution.

Shear Stress [Pa] Creep	Viscosity [Pa s] Creep
27	0.033
15	0.1
9	0.33
6	1
3	33.33
1	250

Shear Stress [Pa] Sweep Tests #1	Viscosity [Pa s] Sweep Tests #1	Shear Stress [Pa] Sweep Tests #2	Viscosity [Pa s] Sweep Tests #2
23.58	0.02106	24.92	0.01921
14.95	0.05802	15.79	0.05419
9.452	0.2422	9.993	0.2198
5.968	1.71	6.309	1.224
3.765	13.93	2.512	38.35
0.9458	317	0.9999	171.9

Figure 28 and table 8, shows samples from the 2.5% wt. Laponite solutions tests. Similar to the 2% solution, the figure shows that the creep viscosity values follow the stress sweep results.

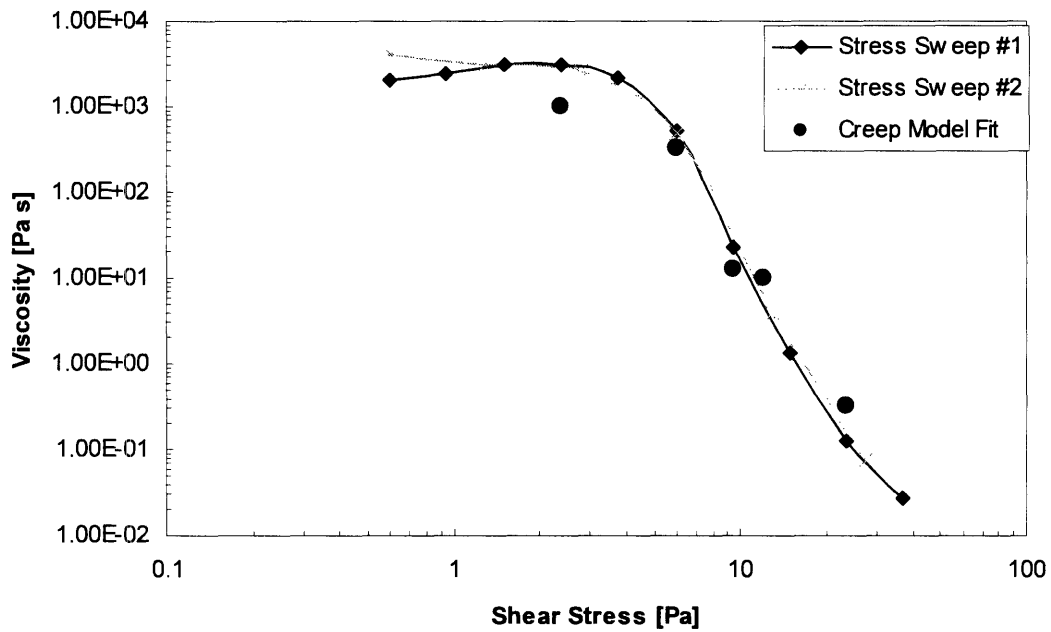


Figure 28: A fit of the creep extracted viscosity values for a 2.5% wt. Laponite solution mapped onto the stress sweep data for the same 2.5% wt. Laponite sample.

Table 8: Viscosity values for both the creep tests and stress sweeps tests at certain shear stresses on the 2.5% wt. Laponite solution.

Shear Stress [Pa] Creep	Viscosity [Pa s] Creep
23.57	0.333
12	10
9.44	12.5
6	333.33
2.374	1000

Shear Stress [Pa] Sweep Tests #1	Viscosity [Pa s] Sweep Tests #1	Shear Stress [Pa] Sweep Tests #2	Viscosity [Pa s] Sweep Tests #2
23.57	0.1288	27.34	0.07412
14.96	1.327	12.83	3.822
9.441	23.07	N/A	N/A
5.957	513.7	5.955	491.8
3.76	2214	2.761	2634

Figure 29 shows the results of the stress sweep tests and the creep tests superimposed onto one graph. The trend lines show the relationship between the yield stresses on a power law curve and on an exponential relationship with respect to Laponite wt. concentration.

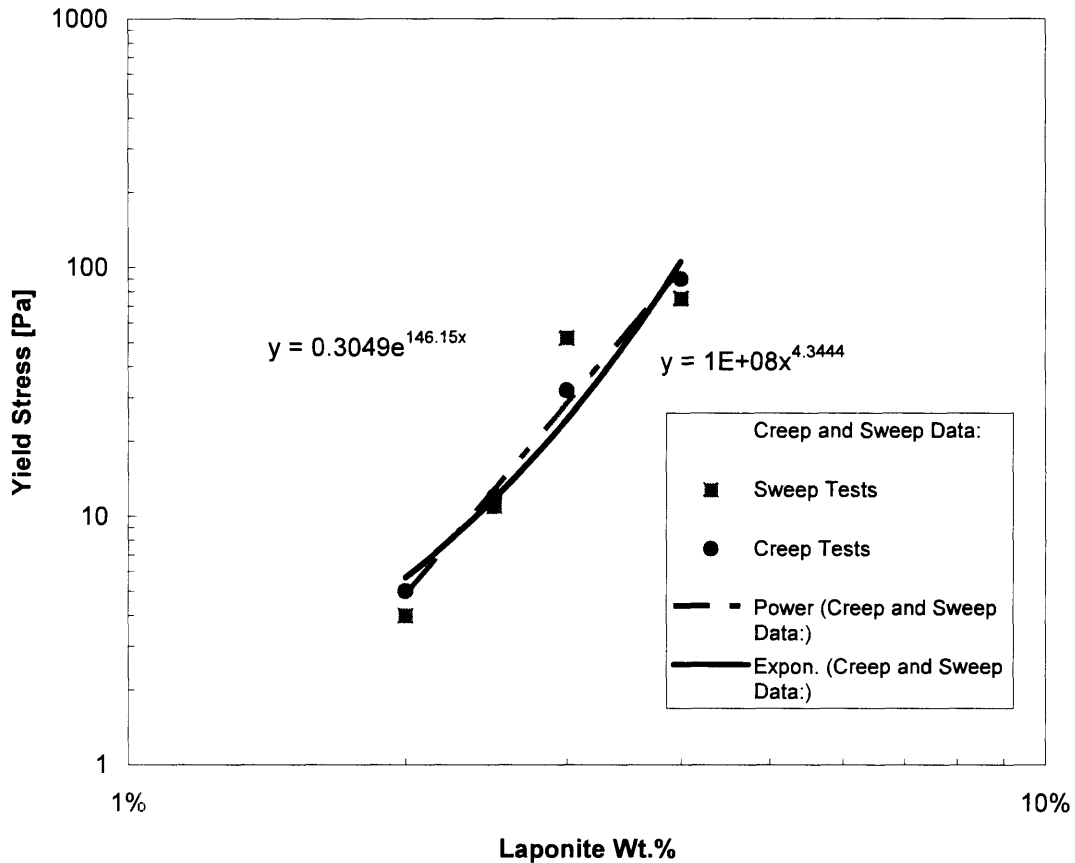


Figure 29: Compendium of all the yield stress points gathered from the stress sweep tests and creep tests for all the 2%, 2.5%, 3%, and 4% wt. solutions of Laponite and also shown is the equation of a fitted power law line and a exponential line corresponding to the yield stresses at a certain Laponite weight concentrations.

5.3 Large Amplitude Oscillatory Shear (LAOS) Tests

After applying an oscillatory shear test and outputting the form in a Lissajous figure of stress and strain, one is able to see a fingerprint of the characteristics of the fluid.

At an oscillatory stress at

$$\sigma_o = \sin(\omega t) \quad (5.1)$$

and the strain response is

$$\sigma_o = \cos(\omega t) \quad (5.2)$$

This shows a 90° phase difference between the input stress and the strain response. In figure 30 a perfect circle denoting a pure linear Newtonian fluid. Figure 31 shows the results from two LAOS tests of the Newtonian fluid of silicone oil. A perfect circle is not visible, since the phase difference is tilted a couple degrees, is this seen in the phase difference plot in figure 31. This phase difference is a result of silicon oil's similar but imperfect Newtonian fluid properties.

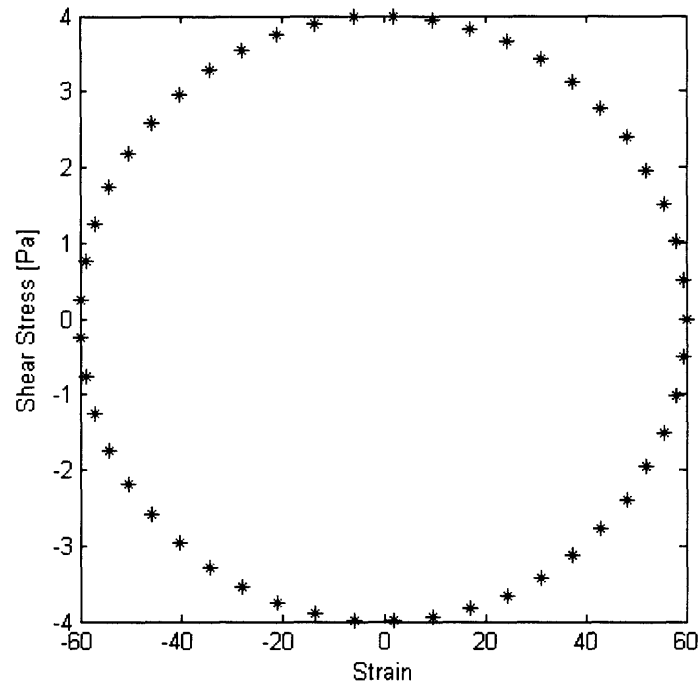


Figure 30: This perfect circle on a Lissajous figure representing a pure Newtonian fluid.

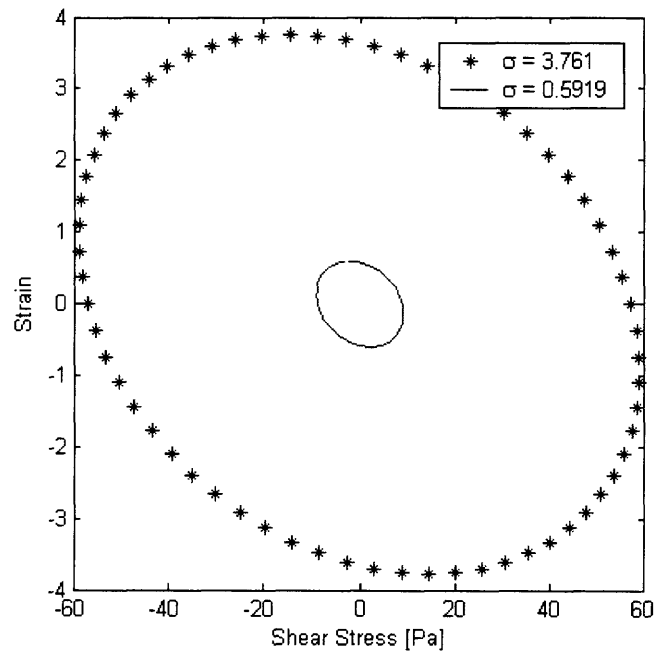


Figure 31: A Lissajous figure of stress and strain of a Newtonian fluid, silicone oil, at input stress amplitudes of 3.761 Pa and 0.5919 Pa, showing that a Newtonian fluid is characterized by a stress input and strain response that is close to a 90° phase difference, showing a fingerprint close to a circle.

Based on the results in figure 31, the phase shift for the 0.5919 Pa sample was 89.94° and for the 3.76a Pa test, the phase shift was 90.11° which explains the imperfect circle in figure 31. Figure 32 shows the phase difference with respect to the oscillation stress, and it can be seen that the data wavers around 90°.

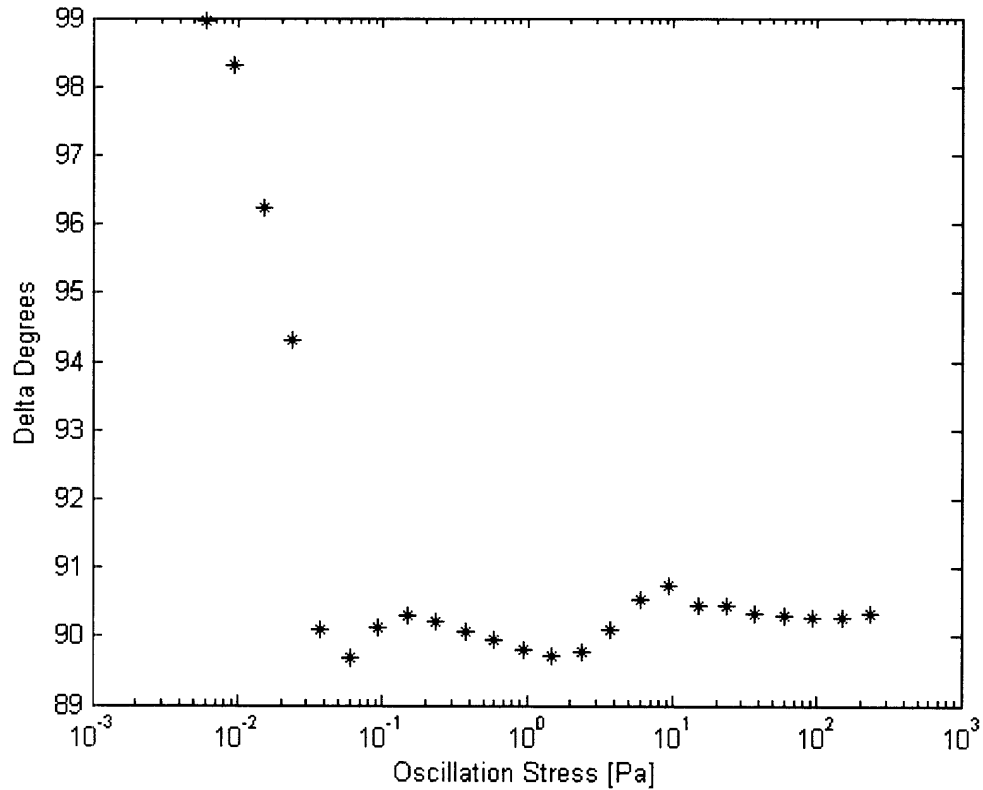


Figure 32: Experimental LAOS data on the silicone oil showing the relationship between the phase degree difference and the oscillation stress.

On the other hand, an elastic solid would give a profile of a straight line on a Lissajous figure of stress and strain. Where given an oscillation stress, there would be very little strain response since the material is a linearly elastic solid. This is seen in figure 33.

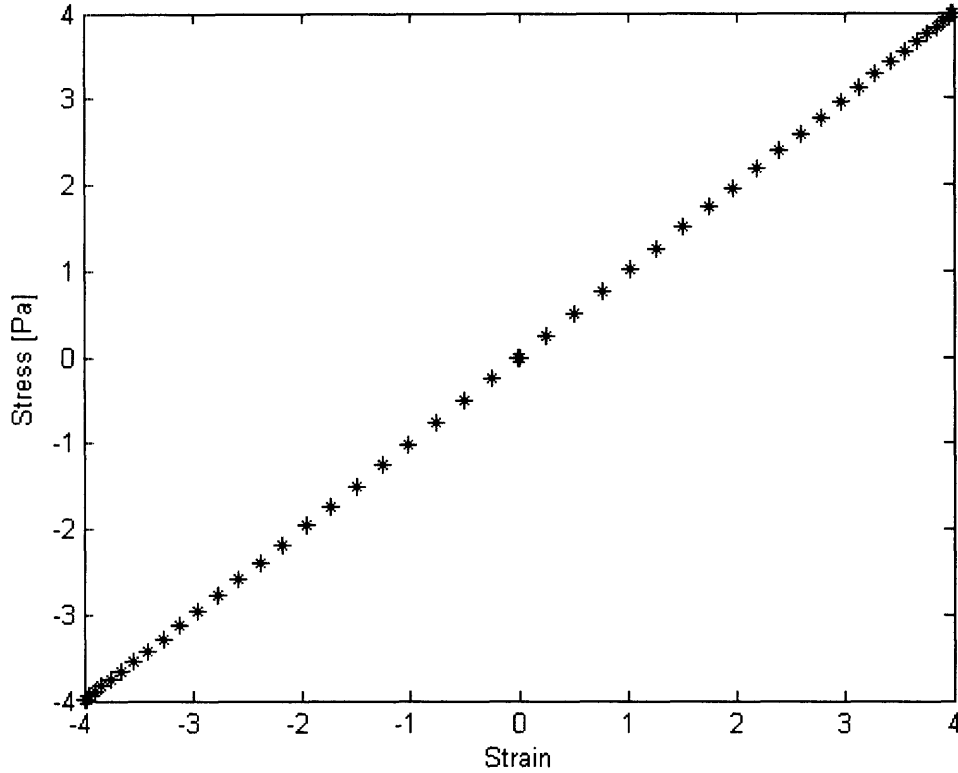


Figure 33: Lissajous figure corresponding to a perfect elastic solid.

When applying the large amplitude oscillatory shear to the Laponite samples at different oscillation stresses there were many different Lissajous figures that characterized the fluid at different stages. In figure 34, a 2% wt. Laponite solution is shown at two different oscillatory stresses on a Lissajous plot, 5.963 Pa and 9.454 Pa, corresponding to an input stress to yield stress ratio, $s = 0.5963$ and $s = 0.9454$. The yield stress as determined by the LAOS test and model, not the stress sweep and creep test. Fitted with that is the model that predicts the shape of the Lissajous figure, as explained in section 4.4. The linear visco-elastic region is shown by the elliptical figure on a Lissajous plot.

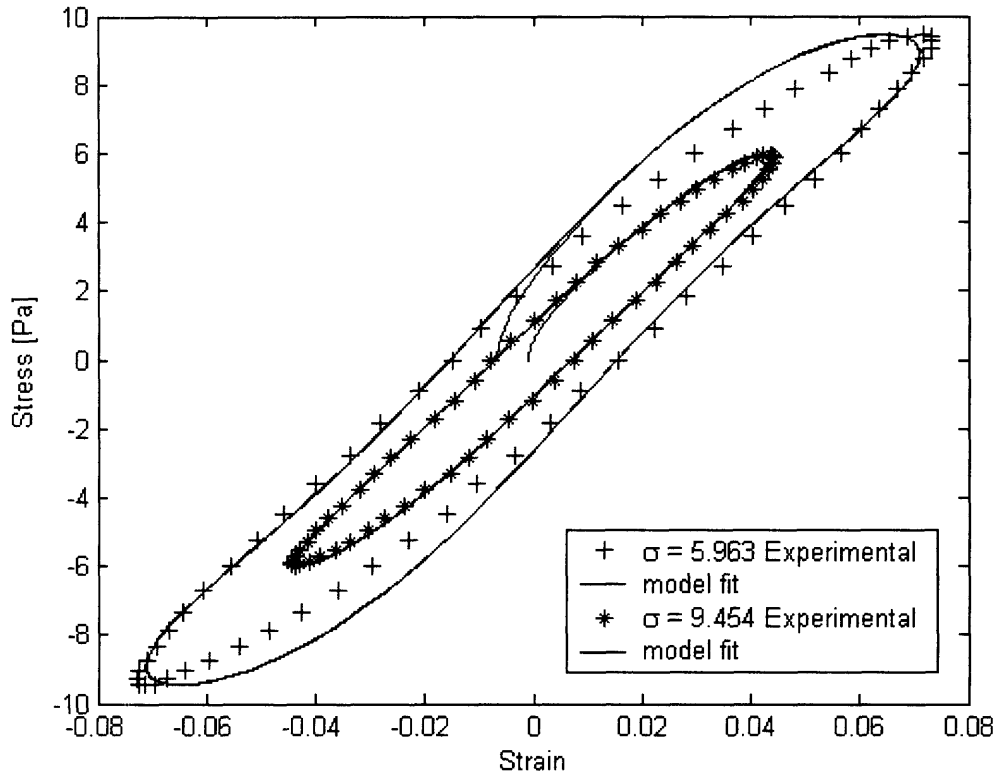


Figure 34: Lissajous figures of 2% wt. Laponite at $s = 0.5963$ and $s = 0.9454$, fit with the model in the linear visco-elastic regime.

As the oscillation stress approaches the yield stress, the Lissajous figure becomes expanded, transforming from an ellipsoid to a parallelogram. This phenomenon is also shown in the LAOS Lissajous fingerprint model. The fitted model with experiment data can be seen in figure 35 at $s = 1.5$.

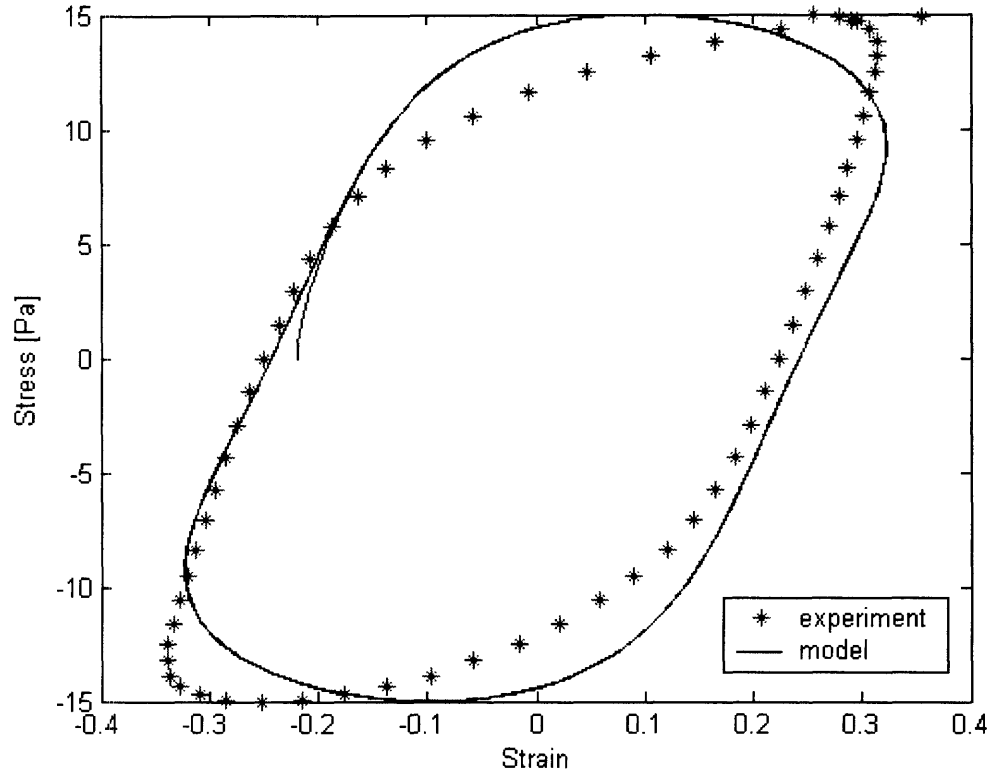


Figure 35: Lissajous figure of 2% wt. Laponite at $s = 1.5$ fit with the model as the oscillation stress exceeds the yield stress of the solution.

When fitting the model to the experimental results there are two main factors to control, τ , the time constant of the fluid and G , the modulus. The table below shows the values used to model the 2% wt. Laponite at specific oscillation stresses.

Table 9: The values used to fit the model to the experimental results of the 2% wt. Laponite LAOS tests.

Input Stress Amplitude, σ_0 [Pa]	Yield Stress, σ_y [Pa]	Time Constant, τ [s]	Modulus, G [Pa]	Frequency, ω [rad/s]
5.963	10	0.25	150	0.628
9.454	10	0.25	175	0.628
14.99	10	0.22	125	0.628

When observing the 2.5% Laponite mixture the results are similar to that of the 2% wt. Laponite solution. Figure 36-37 show the model again fit to the LAOS data obtained from the 2.5% wt. Laponite mixture on stresses ranging from 9.454 Pa to 23.75 Pa to see the entire range of shapes from the linear elastic region to the non-linear region.

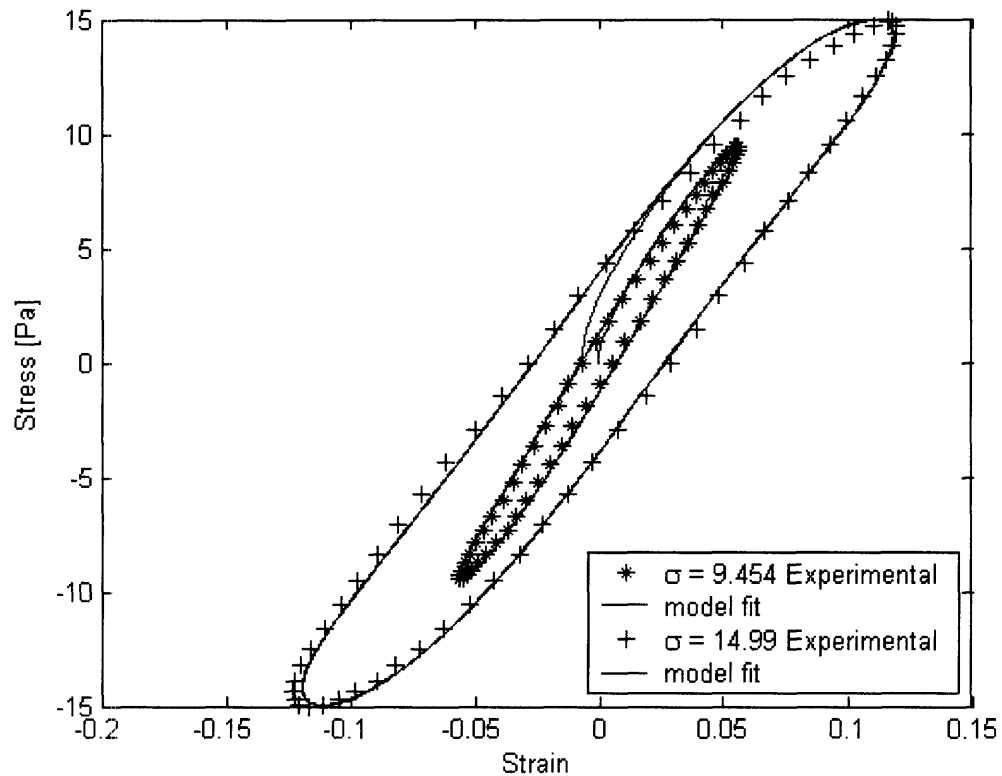


Figure 36: Lissajous figures of 2.5% wt. Laponite at $s = 0.5$ and $s = 0.75$, fit with the model in the linear visco-elastic regime resulting in ellipsoid Lissajous figures.

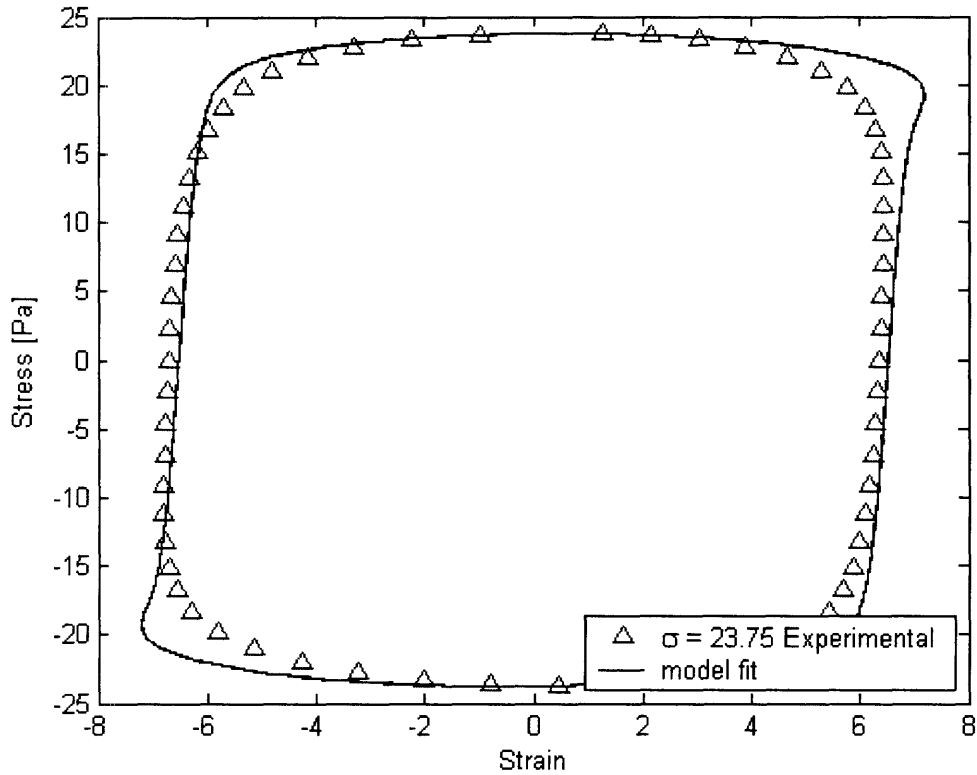


Figure 37: Lissajous figure of 2.5% wt. Laponite at $s = 1.2$ fit with the model as the oscillation stress exceeds the yield stress of the 2.5% wt. Laponite solution.

The tables of values used to fit the 2.5% wt. Laponite experimental results are below in table 10.

Table 10: Values used to fit the model to the experimental results of the 2.5% wt. Laponite.

Input Stress Amplitude, σ_0 [Pa]	Yield Stress, σ_y [Pa]	Time Constant, τ [s]	Modulus, G [Pa]	Frequency, ω [rad/s]
9.454	20	0.2	180	0.628
14.99	20	0.3	150	0.628
23.75	20	0.012	55	0.628

The 3% wt. Laponite and the 4% wt. Laponite show more of the nonlinear characteristics of the Laponite solutions. As the stress increases and comes close to the yield stress of the fluid, one can observe that in the Lissajous figures, the edges start to stray from the ellipsoid shape. This shows that at those oscillation stresses, the Laponite solution is becoming more non-linear. Figure 38, shows the LAOS results of the 3% wt. Laponite solution at 23.75 Pa or $s = 0.4$, where the ellipsoid shape is still retained, and at 37.65 Pa or $s = 0.7$, where the nonlinearity can be start to be seen on the edges of the ellipsoid.

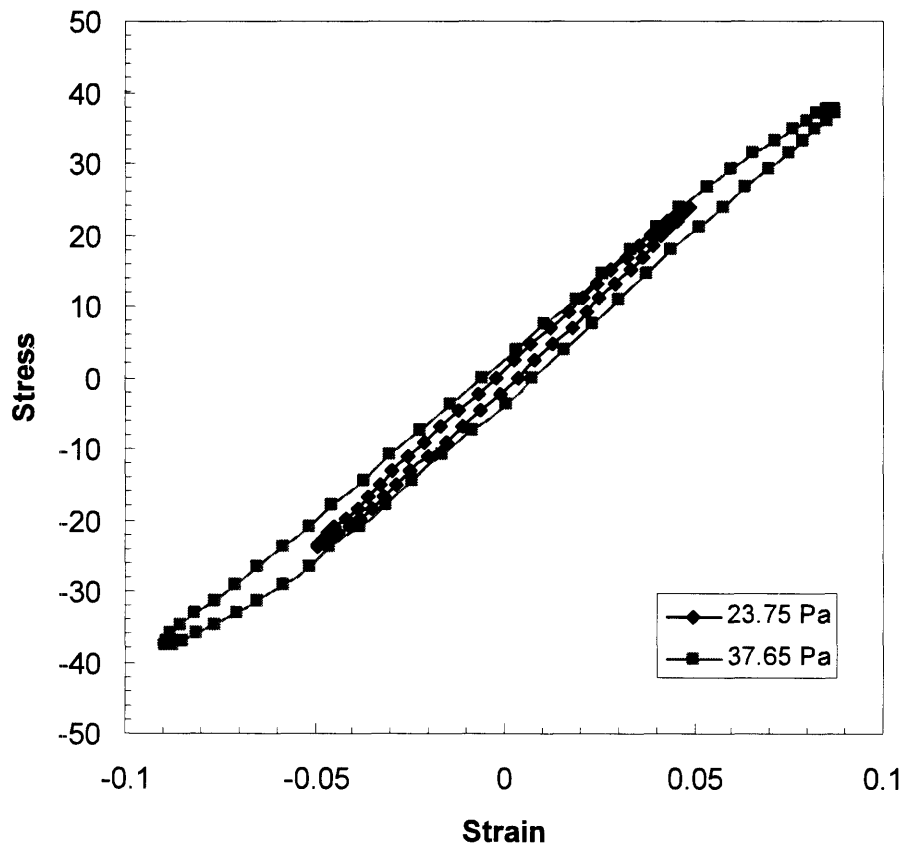


Figure 38: 3% wt. Laponite solution tested at $s = 0.4$ and $s = 0.7$, showing the progression from an ellipsoid shape to a non-linear shape that deforms the ends of the ellipsoid.

The evolution of deformation model also fits the non-linear regions of the Laponite fluid as shown in figure 39. The equations in section 4.4, models the population imbalance of

the defects in the structured fluid and predicts the deformation in the Lissajous figure due to the increasing stress.

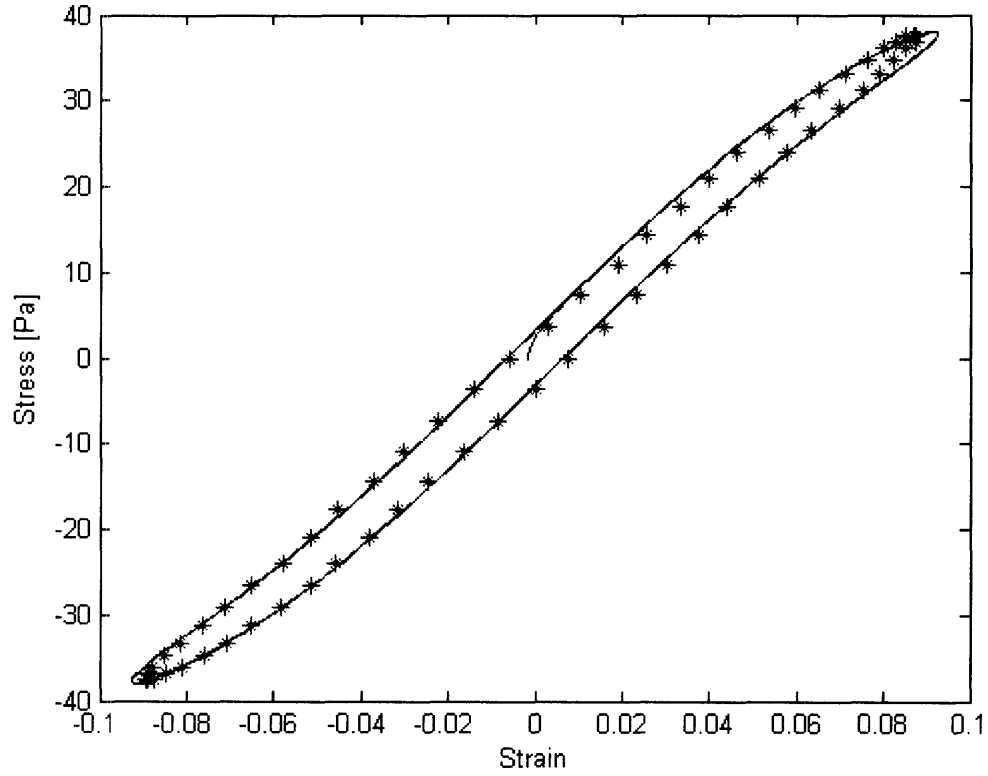


Figure 39: Lissajous figure with both the experimental data and model fit for 3% wt. Laponite as stress was increasing closer to yield stress, showing a nonlinear portion of the fluid at $s = 0.7$.

The values used to fit the LAOS result of the nonlinear 3% wt. Laponite at 37.65 Pa are shown in table 11.

Table 11: Values used to fit the model to the nonlinear experimental results of the 3% wt. Laponite at 37.65 Pa.

Input Stress Amplitude, σ_0 [Pa]	Yield Stress, σ_y [Pa]	Time Constant, τ [s]	Modulus, G [Pa]	Frequency, ω [rad/s]
37.65	55	0.1	500	0.628

In the 4% wt. Laponite solutions, one is able to see the entire transition from a linear ellipsoid shape, to a non-linear skewed ellipsoid shape, to a deformed shape where the input stress exceeds the yield stress of the 4% wt. Laponite solution. Figure 40, shows the linear elasto-plastic regimes of the 4% wt. Laponite fluid at 37.65 Pa ($s = 0.3$), 59.68 Pa ($s = 0.52$), and 94.59 Pa ($s = 0.8$). Figure 41 shows the 94.59 Pa oscillatory stress LAOS data plotted on a Lissajous figure of stress and strain fit with the model to match the deformation in the fluid.

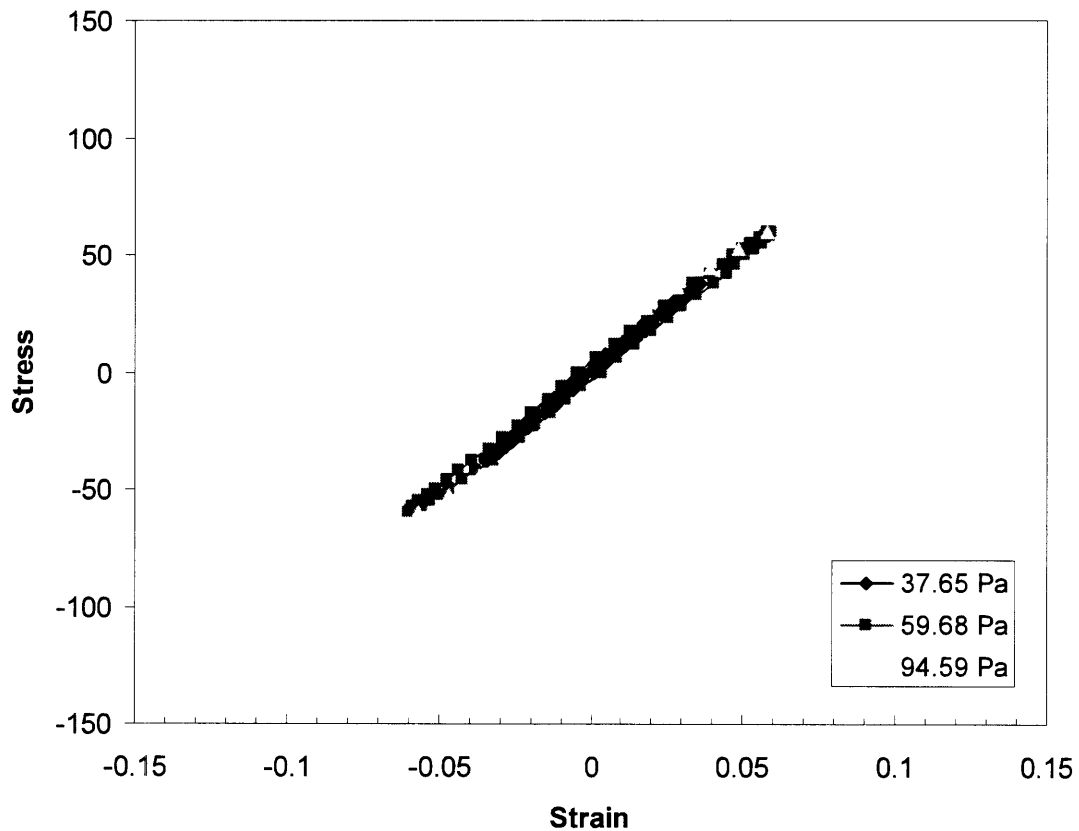


Figure 40: LAOS tests of 4% wt. Laponite solution $s = 0.3$, $s = 0.5$, and $s = 0.8$ showing the transition from a linear ellipsoid to a non-linear skewed ellipsoid on a Lissajous figure of stress and strain.

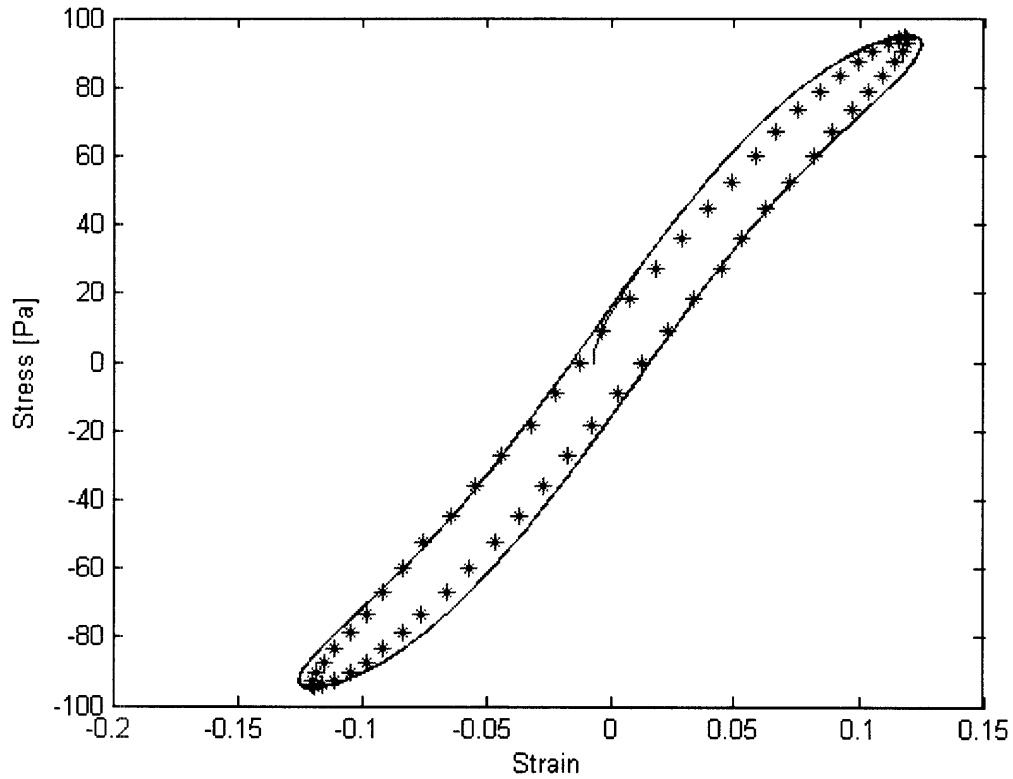


Figure 41: LAOS data of the 4% wt. Laponite at $s = 0.8$, and fit with the same fingerprint in the model to describe the state of deformation in the fluid on a Lissajous figure of stress and strain.

Figure 42-43, combines both graphs above and adds another fit of an input stress above the yield stress to see the evolution of the fingerprints from a perfect ellipsoid, to a skewed ellipsoid with edges moving into the non-linear regime, and finally in the parallelogram shape showing the large changes in deformation rate and accumulated strain [1, 2].

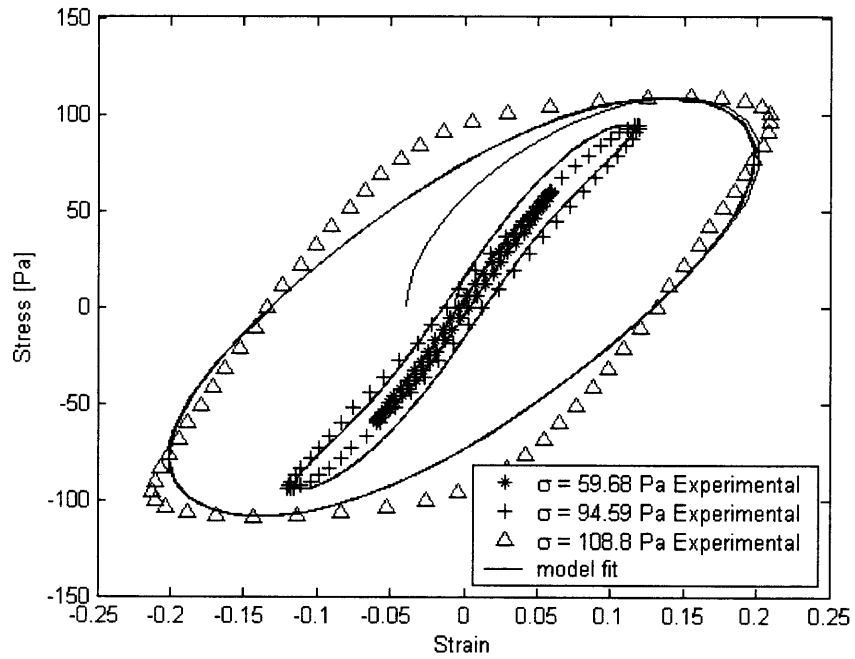


Figure 42: Showing the transition from a linear visco-elastic ellipsoid Lissajous figure to a parallelogram nonlinear Lissajous figure of a 4% wt. Laponite solution by LAOS testing at $s = 0.5$, $s = 0.8$, and $s = 0.95$.

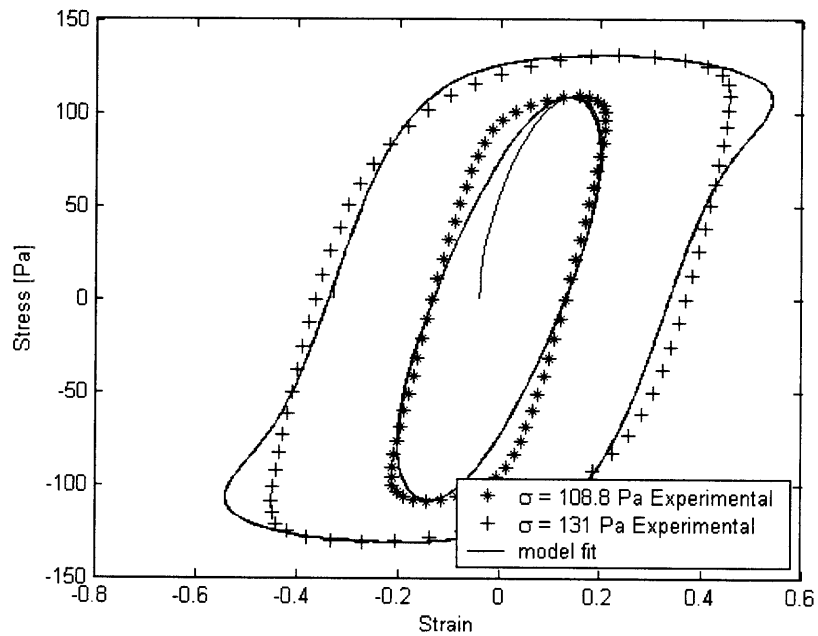


Figure 43: The comparison of Lissajous figures near the yield stress $s = 0.95$, and above the yield stress at $s = 1.1$ fit with the model for tests on the 4% wt. Laponite.

Figure 44 shows G' , the storage modulus and G'' , the loss modulus for oscillation stress sweep and strain sweep tests. At around 100 Pa, one can notice a drop occurs in both G' and G'' with the increase of the phase angle difference. This area is where the fluid has been yielded.

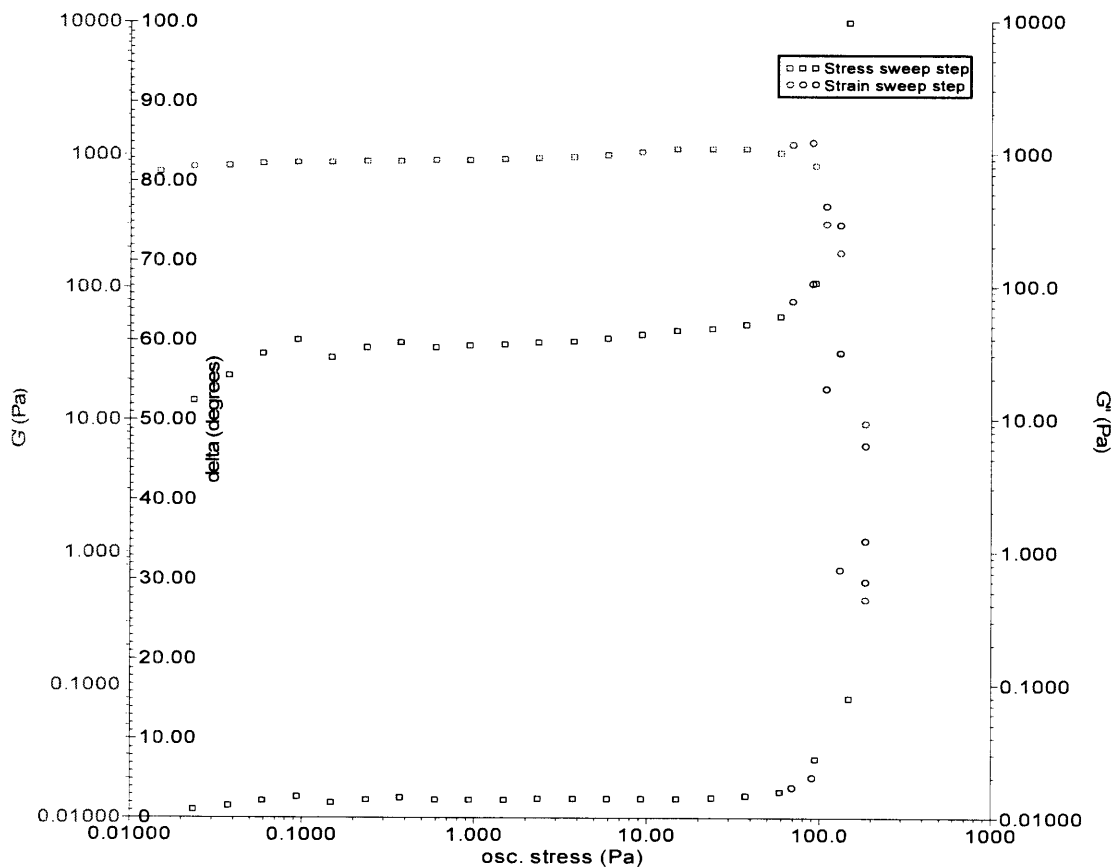


Figure 44: Storage modulus, G' , loss modulus, G'' , and delta plotted with respect to the oscillation stress for a 4% wt. Laponite solution to see where the yielding occurred on the solution.

Figures 45-46 shows the corresponding waveforms of stress and strain responses to $s < 1$ and $s > 1$ on the LAOS tests on the %4 wt. Laponite. The waveform of $s < 1$ shows the two oscillations in phase, while the accumulation of deformation and change of phase angle is clearly visible in the waveform of $s > 1$.

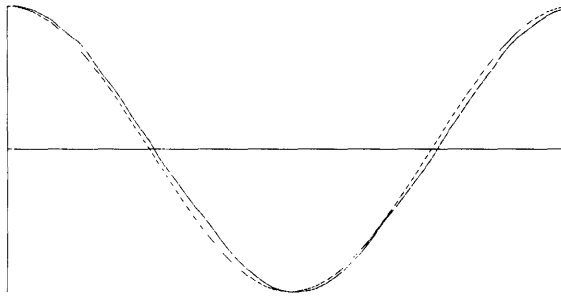


Figure 45: Waveform showing no phase difference between the applied stress and strain response on a 4% wt. Laponite solution at $s < 1$.

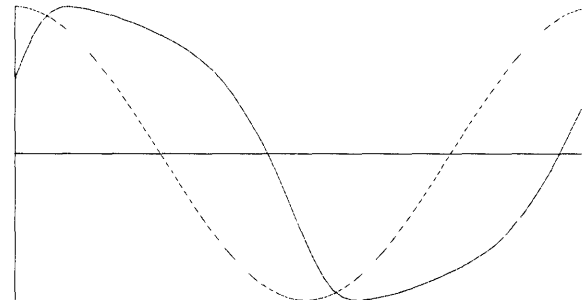


Figure 46: Waveform of a 4% wt. Laponite solution at $s > 1$, showing the deformation and phase difference of the strain response to the applied stress.

The nonlinearity of the LAOS plots as the input stress approaches and exceeds the yield stress corresponds to the energy dissipated in the deformations and accumulated strain [16]. To compare the values used in the simulation model to the values extracted from the 4% wt. Laponite results can be seen in table 12 below.

Table 12: Values used to fit the model to the experimental LAOS results of the 4% wt. Laponite solution.

Input Stress Amplitude, σ_0 [Pa]	Yield Stress, σ_y [Pa]	Time Constant, τ [s]	Modulus, G [Pa]	Frequency, ω [rad/s]
59.68	115	0.1	1110	0.628
14.99	115	0.15	1025	0.628
108.8	115	1	500	0.628
131	115	.07	800	0.628

When comparing all the yield stresses obtained in the stepped stress sweep tests and the creep tests, with Lissajous fingerprints exhibiting non-linear characteristics corresponding to the oscillation stress on the LAOS tests and the fitted model, one can see in table 13, that the yield stresses values are comparable. The yield stress value from the LAOS tests is the value closest to the yield where a clear data point was obtained. Therefore, it is a slight higher value than the yield stresses as characterized by the stress sweep tests or creep tests. The yield stresses on the deformation model, is one that gave a good fit to the LAOS Lissajous figures.

Table 13: Comparing yield stress values from 2%, 2.5%, 3%, and 4% Laponite samples from the stepped stress sweeps and creep tests, with the oscillation stresses corresponding to the non-linear Lissajous figures from the LAOS tests and from the model.

Concentration	Yield Stress Stress Sweep	Yield Stress Creep Test	Yield Stress LAOS Tests	Yield Stress Model
2%	4 Pa	5 Pa	15 Pa	10Pa
2.5%	11 Pa	12 Pa	23 Pa	20 Pa
3%	52 Pa	32 Pa	38 Pa	55 Pa
4%	75 Pa	90 Pa	109 Pa	115 Pa

Chapter Six

Conclusion

The goal of this thesis was to first gain a basic understanding of the methods and analysis used in Rheology. Studying the phenomenon of yield stress, the complexities of Laponite, and slug locomotion, a basic scope was obtained for the project. Then by applying stepped stress sweeps and creep tests, basic and fundamental rheological data was obtained and analyzed. The stepped stress sweeps helped to first categorize the concentrations of Laponite as yield stress fluids or not, and the creep tests verified those results. The stepped stress sweeps categorized the 2%, 2.5%, 3%, and 4% wt. Laponite concentrations as fluids with yield stresses. The creep tests verified the viscosity values, as well as the yield stresses from viewing the differences in Compliance $J(t)$ data on whether the fluid response was that when applied a shear stress above or below the yield stress. Those concepts then were translated when applying large amplitude oscillatory shear tests on to the Laponite concentrations. Through the LAOS tests, the results were plotted onto Lissajous figures of stress and strain, and specific fingerprints of characteristics were seen at different input stress to yield stress ratios, $s = (\sigma_o / \sigma_y)$. At $s < 1$, the rheological fingerprint would resemble an ellipsoid shape, giving information that the fluid is in the linear elasto-plastic regime. As s approached 1, the nonlinearities would be visible with an ellipsoid shape growing outward with the ends starting to become skewed. When the input stress exceeded the yield stress, at $s > 1$, the Lissajous figure would start to resemble a parallelogram to show the accumulated strain and deformation. The LAOS results were fit to a model of the evolution deformation in the fluid. This model matched the data well.

After characterizing the Laponite fluid concentrations and observing slug slime, an emulation process to create a artificial slug slime is possible. Looking at the properties of

slug slime in table 14, one can notice that the yield stress is a bit higher than characterized by the concentrations of Laponite so far. The viscosity after yield values for Laponite are also magnitudes below the slug slime. The heal time, though not qualitatively measured, quantitatively the 4% wt. solution is sufficient for that heal time value.

Table 14: Slug slime properties.

Yield Stress	Viscosity After Yielding	Heal Time
~ 400Pa – 500 Pa	~ 5 Pa	< 1 second

From this point, with the Laponite solutions characterized, one might want to increase the yield stress by testing higher concentrations of Laponite solutions, say a 5% wt. solution. Then by adding various polymers, more alterations in the fluid properties can be made to fit the viscosity after yielding values.

Laponite solutions are used in a variety of applications. Through this characterization of Laponite in the various analyses and tests, a model to emulate slug slime is established and by adding polymer one can eventually create a solution matching the properties of slug slime, in order to further understand the complexities and uses of slug locomotion. Slug locomotion is an unique type of movement and potentially has many practical applications. As nature is the most efficient engineering design on the planet, it is only appropriate that research can be done to understand and then emulate those designs that may be used to help in positively affecting people.

References

1. Guo, J., et al. *Rheological Fingerprinting of Nonlinear (Yield Stress) Materials by Large Amplitude Oscillatory Shear*. in *The XIVth International Congress on Rheology*. 2004. Seoul, Korea.
2. Deshmukh, S.S. and G. McKinley. *Rheological Behavior of Magnetorheological Suspensions under Shear, Creep, and Large Amplitude Oscillatory Shear (LAOS) flow*. in *The XIVth International Congress on Rheology*. 2004. Seoul, Korea.
3. Barnes, H.A., J.F. Hutton, and K. Walters, *An introduction to rheology*. 1989, Amsterdam ; New York: Elsevier : Distributors for the U.S. and Canada Elsevier Science Pub. Co. ix, 199.
4. Barnes, H.A., *The yield stress - a review or 'pi alpha nu tau alpha rho epsilon iota' - everything flows?* *Journal of Non-Newtonian Fluid Mechanics*, 1999. **81**(1-2): p. 133-178.
5. Papanastasiou, T.C., *Flows of Materials with Yield*. *Journal of Rheology*, 1987. **31**(5): p. 385-404.
6. Dekee, D. and C.F.C.M. Fong, *A True Yield Stress*. *Journal of Rheology*, 1993. **37**(4): p. 775-776.
7. *Laponite Science*. 2005, Laponite.com.
8. Zebrowski, J., et al., *Shake-gels: shear-induced gelation of laponite-PEO mixtures*. *Colloids and Surfaces a-Physicochemical and Engineering Aspects*, 2003. **213**(2-3): p. 189-197.

9. *Laponite Technical Information L204/01g*. 2005, Rockwood Additives Limited.
10. *Laponite Applications*. 2005, Laponite.com.
11. Chan, B., N.J. Balmforth, and A.E. Hosoi, *Building a better snail: Lubrication and adhesive location*. In review.
12. Chan, B., et al. *Mechanical Devices for Snail-like Locomotion*. in *World Congress on Biomimetics, Artificial Muscles and Nano-Bio*. 2004.
13. Richter, K.O., *Aspects of Nutrient Cycling by Ariolimax-Columbianus (Mollusca, Arionidae) in Pacific Northwest Coniferous Forests*. *Pedobiologia*, 1979. **19**(1): p. 60-74.
14. Rollo, C.D., *Consequences of Competition on the Reproduction and Mortality of 3 Species of Terrestrial Slugs*. *Researches on Population Ecology*, 1983. **25**(1): p. 20-43.
15. Gordon, D.G. and Western Society of Malacologists., *Field guide to the slug*. Sasquatch field guide series. 1994, Seattle: Sasquatch Books. 48 p.
16. Citerne, G.P., P.J. Carreau, and M. Moan, *Rheological properties of peanut butter*. *Rheologica Acta*, 2001. **40**(1): p. 86-96.
17. Mourchid, A., et al., *Phase-Diagram of Colloidal Dispersions of Anisotropic Charged-Particles - Equilibrium Properties, Structure, and Rheology of Laponite Suspensions*. *Langmuir*, 1995. **11**(6): p. 1942-1950.
18. Denny, M.W. and J.M. Gosline, *The Physical-Properties of the Pedal Mucus of the Terrestrial Slug, Ariolimax-Columbianus*. *Journal of Experimental Biology*, 1980. **88**(OCT): p. 375-393.

19. Denny, M.W., *Mechanical-Properties of Pedal Mucus and Their Consequences for Gastropod Structure and Performance*. *American Zoologist*, 1984. **24**(1): p. 23-36.

Appendix : Matlab Code Used to Fit LAOS

Results on Lissajous Figures

1st Matlab script. Calls on the second script “equation.m” to solve the coupled non-linear ordinary equations for the evolution of the deformation of a yield stress characteristic fluid and outputs a Lissajous figure of stress and strain.

```
% Douglas Hwang
% Class of 2005, Mechanical Engineering
% Undergraduate Thesis
% Advisor: Professor Gareth McKinley

% Matlab script outputs graphs of stress, strain, and delta
% Outputs a lissajous figure of stress and strain
% Using a second script to model and solve the non-linear coupled
% differential equations.

% Global Variables
global tau G sigma_y sigma_knot omega

% Input Variables
omega = 0.628;      %frequency [rad/s]
G = 150;           %modulus [Pa]
tau = 1;           %time constant [s]
sigma_knot = 95;   %input stress amplitude [Pa]
sigma_y = 115;     %yield stress [Pa]

C2 = 2*pi/omega;   %specifies a period

% Initial conditions for the differential equations
Y0 = [0 0];

% Ordinary Differential Equation (ODE) parameters
n = 4;             %Number of cycles
T1 = n*C2;        %Number of periods
Tspan = [0 T1];   %Specifies an interval of integration

% Uses the script "equation.m" to solve the ODEs
[tout, yout] = ode45('equation',Tspan,Y0);

% Function Definitions
stress = sigma_knot*sin(omega*tout);
strain = yout(:,1);
delta = yout(:,2);
```

```

%Offset correction on the Lissajous figures
offset = (max(strain)+min(strain))/2;
strain = strain - offset;

%Plots of stress, strain, and delta with respect to time
figure(1), plot(tout, stress), title('stress vs
tout'), xlabel('time'), ylabel('stress')
figure(2), plot(tout, strain), title('strain vs tout'),
xlabel('time'), ylabel('strain')
figure(3), plot(tout, delta), title('delta vs tout'), xlabel('time'),
ylabel('delta')

%Plots a Lissajous figure of stress and strain
figure(1), plot(strain, stress), title('Stress vs
Strain'), xlabel('Strain'), ylabel('Stress [Pa]')

```

2nd Matlab script used in the first script as a function which is called on to solve the ODEs.

```

%Function code to solve the differential equations of strain and delta
%Takes two parameters, Tspan and the initial conditions
function dydt = eqnc(t,y)

%Global Variables
global tau G sigma_y sigma_knot omega C2

%Function Initialization
e = y(1);
delta = y(2);
sigma = sigma_knot*sin(omega*t);

%Differential Equations of Strain and Delta
dgamma_dt = (1/(tau*G))*(sigma - G*delta);
ddelta_dt = dgamma_dt * (1 - ((G*sigma*delta)/(sigma_y^2)));

%Output
dydt = [dgamma_dt; ddelta_dt];

```

